Composition and Conformation of Hetero- versus Homo-Fluorinated Triazolamers Influence their Activity on Islet Amyloid Polypeptide Aggregation

José Laxio Arenas, Jacopo Lesma, Tap Ha-duong, Bikash Ranjan Sahoo, Ayyalusamy Ramamoorthy, Nicolo Tonali, Jean-louis Soulier, Frédéric Halgand, François Giraud, Benoît Crousse, et al.

Chemistry–A European Journal
Research Article
doi.org/10.1002/chem.202303887
Chemistry Europe
European Chemical Societies Publishing
www.chemeurj.org

Composition and Conformation of Hetero- *versus* Homo-Fluorinated Triazolamers Influence their Activity on Islet Amyloid Polypeptide Aggregation

José Laxio Arenas,[a] Jacopo Lesma,[a] Tap Ha-Duong,[a] Bikash Ranjan Sahoo,[b] Ayyalusamy Ramamoorthy,[b] Nicolo Tonali,[a] Jean-Louis Soulier,[a] Frédéric Halgand,[c] François Giraud,[d] Benoît Crousse,[a] Julia Kaffy,*[a] and Sandrine Ongeri*[a]

Novel fluorinated foldamers based on aminomethyl-1,4-triazol-yl-difluoroacetic acid (1,4-Tz–CF_2) units were synthesized and their conformational behaviour was studied by NMR and molecular dynamics. Their activity on the aggregation of the human islet amyloid polypeptide (hIAPP) amyloid protein was evaluated by fluorescence spectroscopy and mass spectrometry. The fluorine labelling of these foldamers allowed the analysis of their interaction with the target protein. We demonstrated that the preferred extended conformation of homotriazolamers of 1,4-Tz–CF_2 unit increases the aggregation of hIAPP, while the hairpin-like conformation of more flexible heterotriazolamers containing two 1,4-Tz–CF_2 units mixed with natural amino acids from the hIAPP sequence reduces it, and more efficiently than the parent natural peptide. The longer heterotriazolamers having three 1,4-Tz–CF_2 units adopting more folded hairpin-like and ladder-like structures similar to short multi-stranded β-sheets have no effect. This work demonstrates that a good balance between the structuring and flexibility of these foldamers is necessary to allow efficient interaction with the target protein.

Introduction

Misfolded protein aggregation into β-sheet rich amyloid fibrils is associated with more than 20 human diseases which include Alzheimer's (AD), Parkinson's (PD) diseases, and type II diabetes (T2D).[1–3] T2D is a major public health issue, affecting around 400 million people worldwide. This number is expected to exceed half a billion by 2045, while no causal treatment for this disease is available.[4,5] Human islet amyloid polypeptide (hIAPP, also known as amylin) aggregation is involved in the death of pancreatic β-cells of T2D patients, by a very partially understood mechanism. hIAPP undergoes a conformational change inducing an aggregation pathway providing toxic soluble oligomers and fibers.[6–8] The aggregated species adopt β-sheet rich conformations and amyloid deposits are found in the pancreas of more than 95% of diabetic patients.[6–8] Preventing both the presence of soluble transient oligomers and late aggregated forms of hIAPP is crucial to prevent the cell toxicity that is caused by membrane disruption and also by other less understood phenomena induced by hIAPP aggregation.[9–11] This strategy has to be explored to consider a viable therapy against T2D. Some small molecules have been reported as inhibitors of hIAPP aggregation, such as polycyclic and polyphenols.[12–15] They often present the disadvantage of being not selective, thus inducing side effects. Few rationally designed peptide derivatives have been reported.[16–19] Foldamer science[20–22] has recently provided original solutions to address some of the peptide issues.[23,24] Their ability to mimic the secondary structure of proteins combined with an increase of stability, selectivity, and membrane permeability afford remarkable new opportunities. Nevertheless, this field is still in its infancy for application as modulators of amyloid protein aggregation. The group of Miranker has reported that helical oligopyridine and oligoquinoline foldamers interfere with the early folding steps of both $A\beta_{1-42}$ (involved in AD)[25,26] and hIAPP[27,28] peptides. Some of us demonstrated that a foldamer composed of six units of 4-amino(methyl)-1,3-thiazole-5-carboxylic acid (ATC) acts as a dual inhibitor of hIAPP and $A\beta_{1-42}$ aggregation and preserves monomeric species.[29] Some of us also recently reported the use of diaza-peptide foldamers to decrease $A\beta_{1-42}$ aggregation.[30] We currently aim to explore the interest of fluorinated foldamers. The design of this new class of foldamers

[a] Dr. J. Laxio Arenas, Dr. J. Lesma, Prof. T. Ha-Duong, Dr. N. Tonali, Dr. J.-L. Soulier, Dr. B. Crousse, J. Kaffy, Prof. S. Ongeri
Université Paris-Saclay, CNRS, BioCIS, Bat. Henri Moissan, 17 av. des Sciences, 91400 Orsay, France
E-mail: sandrine.ongeri@universite-paris-saclay.fr
Julia.kaffy@universite-paris-saclay.fr
[b] Dr. B. Ranjan Sahoo, Prof. A. Ramamoorthy
Biophysics, Department of Chemistry, Biomedical Engineering, Michigan Neuroscience Institute, Macromolecular Science and Engineering, University of Michigan, Ann Arbor, MI 48109-1055, USA
[c] Dr. F. Halgand
Université Paris-Saclay, CNRS, Institut de Chimie Physique, 91405, Orsay, France
[d] F. Giraud
Equipe Biologie et Chimie Structurales, Dept Chimie et Biologie Structurales et Analytiques, ICSN, CNRS, Université Paris Saclay, 1 avenue de la terrasse, 91190 Gif sur Yvette, France

Supporting information for this article is available on the WWW under https://doi.org/10.1002/chem.202303887

has still been poorly addressed by chemists,[31–36] and they are completely unknown as potential modulators of amyloid aggregation or even more widely in the vast field of medicinal chemistry. They could be all the more promising since fluorinated molecules constitute almost 30% of all newly approved drugs[37,38] and the introduction of fluorinated amino-acids into peptides and proteins has been shown to increase their biological activity, their chemical and enzymatic stability as well as a propensity for secondary structure.[23,39–42]

In the present work, we study the conformational preferences and activity on amyloid protein aggregation of novel fluorinated foldamers based on aminomethyl-1,4-triazolyl-difluoroacetic acid (1,4-Tz–CF_2) units. We previously described the insertion in pseudotripeptides of this 1,4-Tz–CF_2 constrained scaffold that can be considered as an analogue of the Gly-difluoroGly dipeptide.[43] The stabilizing electrostatic interactions between the fluorine atoms and the neighboring triazole and the NH of the successive amino acid induced extended conformation. Then we performed the self-assembly of this architecture and carried out conformational studies of these new foldamers (Figure 1, compounds **1**, **2**).[44] Oligomers of 1,4-Tz, called triazolamers, have been rarely reported in literature, especially in medicinal chemistry. Triazoles act as *trans*-amide mimetics with higher stability to hydrolysis. They are easily available thanks to copper(I) catalysed azide-alkyne cycloaddition (CuAAC), which was described independently by the groups of Meldal and Sharpless in 2002.[45,46] Conformational influence of 1,4-Tz has been rarely described until recently. Small bivalent peptidomimetics based on 1,4-Tz adopt rotation-like conformations that replace dipeptide in an α-helical secondary structure.[47,48] In addition, in tri and pentapeptide, the tendency of Tz amino acid to induce β-turn formation has been reported.[49,50] Extended[51–53] or folded[51,54] conformation of peptidotriazolamers have been also reported. Our fluorinated homotriazolamers based on the assembly of tri and four 1,4-Tz–CF_2 adopt elongated β-strand-like structures.[44] Herein we present the rational design, synthesis, and conformational studies of new fluorinated foldamers based on 1,4-Tz–CF_2 mixed with natural amino acids, which we call heterotriazolamers (Figure 1, compounds **3**–**7**). Their conformation preferences and ability to modulate the hIAPP aggregation process have been compared with our previous homotriazolamers (Figure 1, compounds **1**–**2**). We have also introduced the 1,4-Tz–CF_2 unit in flexible β-hairpin like structures based on a piperidine-pyrrolidine β-turn inducer to obtain fluorinated analogues of our recently reported inhibitors of hIAPP aggregation (Figure 1, compounds **8**–**9**).[55] To assess their influence on hIAPP aggregation and conformation, we have combined Thioflavin-T (Tht) kinetic assays, native and ion mobility mass spectrometry (MS), as well as NMR foldamer-hIAPP interaction experiments.

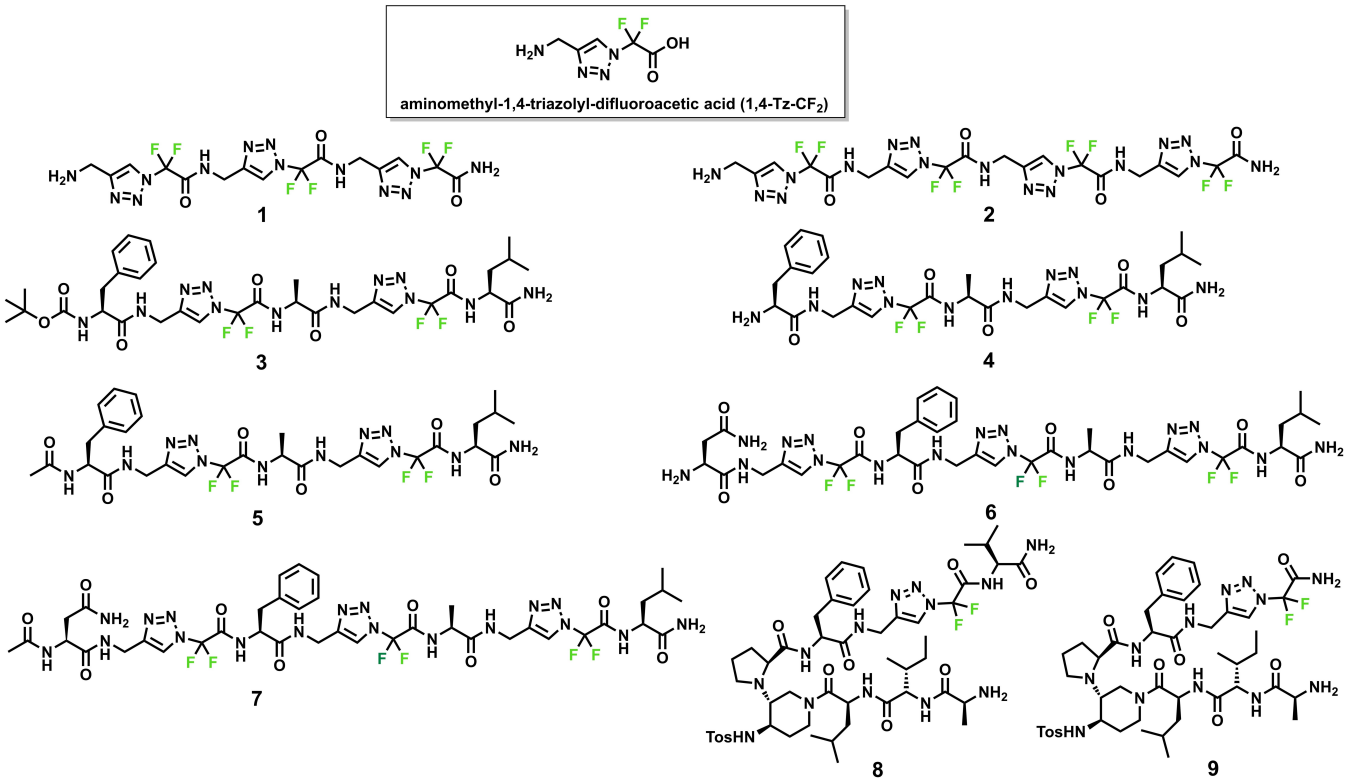

Figure 1. Synthesized and studied fluorinated foldamers based on aminomethyl-1,4-triazolyl-difluoroacetic acid (1,4-Tz–CF_2): homotriazolamers **1** and **2**, heterotriazolamers **3**–**7** and β-hairpin-like compounds **8** and **9**.

Results and Discussion

Design and Synthesis

Our hypothesis is based on the design of extended fluorinated foldamers using 1,4-Tz–CF_2 as a constrained dipeptide mimic. These foldamers could act as β-sheet breakers with respect to β-sheet rich oligomers and fibers of hIAPP, by interacting with hIAPP sequences and forming locally β-sheet structures with these sequences, and consequently disrupting the intra and intermolecular interactions involved in the misfolding and the aggregation processes.[56–59] As mentioned above, we have shown the preferential adoption of extended conformation of homotriazolamers of 1,4-Tz–CF_2 unit.[44] To go further, now we have based the design of new fluorinated foldamers on the hIAPP amyloidogenic sequence N_{21}NFGAIL$_{27}$. Experimental and *in silico* models of monomers and aggregates have shown a critical role in the fibril formation of this region.[56–59] Peptides S_{20}NNFGAILSS$_{29}$, F_{23}GAIL$_{27}$, and N_{21}NFGAIL$_{27}$ based on this sequence have been described to readily form amyloid fibrils.[60,61] The latter has been characterized by X-ray crystallography.[62] Furthermore, this sequence has been described as a promoter of hIAPP fibrils formation[63] or as an inhibitor when introduced in a macrocycle peptide derivative.[64] More recently, hIAPP-derived 21-residues peptides, based on FGAIL sequence, were reported by Kapurniotu et al. as inhibitors of hIAPP and Aβ_{1-40} aggregation.[65–67] In our hands, FGAIL and AIL were inserted in dynamic β-hairpin like structures built on a piperidine-pyrrolidine β-turn inducer to efficiently reduce hIAPP self-assembly.[55] Therefore, we chose to insert some amino acids from this sequence in heterotriazolamers, to further selectively interact with the amyloidogenic sequence of hIAPP, thanks to the specific amino acid lateral chains, while the 1,4-Tz–CF_2 units will act as β-sheet breaker elements. For that purpose, in our first foldamers **3**–**5**, we inserted two difluorotriazole units in the F_{23}GAIL$_{27}$ sequence to obtain three F-(1,4-Tz–CF_2)–A–(1,4-Tz–CF_2)–L derivatives, differing only by their *N*-terminus N–Boc (compound **3**), NH_2 (compound **4**) or AcNH (compound **5**). In order to potentially increase the interactions with hIAPP, we increased the size of our foldamers N-(1,4-Tz–CF_2)–F–(1,4-Tz–CF_2)–A–(1,4-Tz–CF_2)–L **6** and **7**, by inserting three 1,4-Tz–CF_2 in the sequence N_{21}NFGAIL$_{27}$ and having a N-terminal NH_2 (compound **6**) or AcNH (compound **7**). Finally, the 1,4-Tz–CF_2 unit was introduced in flexible β-hairpin like structures based on a piperidine-pyrrolidine β-turn inducer. We designed the direct fluorinated analogues **8** and **9** of our recently reported inhibitors of hIAPP aggregation, bearing AIL et FLV peptide arms (the core of two SREs of hIAPP, F_{15}LVHSS$_{20}$ and N_{22}FGAIL$_{27}$, see reference 55 for the design), linked to the β-turn mimic.[55] We kept the AIL peptide at the N-terminus and replaced FLV with F-(1,4-Tz–CF_2)–V and F-(1,4-Tz–CF_2) at the C-terminus (Figure 1, compounds **8** and **9**, respectively).

The synthesis of our fluorinated heterotriazolamers was based, first on the preparation of 1,4-Tz–CF_2 building blocks bearing one or two amino acids, and secondly on their coupling (Scheme 1). For the first foldamers, we started by coupling the Boc-protected L-phenylalanine and L-arginine with propargylamine in order to obtain Boc-protected amino acids propargylamide **10** and **11**. All difluorinated azides bearing amino acid residues (Alanine, Phenylalanine, and Leucine for **12**, **13**, and **14**, respectively) were obtained following the method described in our previous work, from the direct amidification of ethyl 2-azido-2,2-difluoroacetate with the corresponding amino acids (see SI).[43] Propargylamides and difluoro-azides were put under click chemistry conditions using $CuSO_4.5H_2O$ as a copper source, sodium ascorbate as a reducer of Cu(II) species, and tris(benzyltriazolylmethyl)amine (TBTA) as a ligand to stabilize Cu(I), in a mixture of MeOH/H_2O. The *N*-difluoromethyl-triazole building blocks bearing one (**17**, **18**) or two (**15**, **16**) amino acids were obtained in good yields (60–81%). Building block **15** was submitted to hydrogenolysis (following McMurray methodology using triethylsilane and palladium on carbon in MeOH to generate hydrogen *in situ*[68]) and **17** was treated by a chlorohydric acid solution in dioxane, to obtain respectively the free carboxylic acid and amine intermediates, that were coupled to give compound **3**. The coupling conditions using EDC.HCl, HOBt in the presence of DIPEA in DMF for 48 hours allowed the obtention of **3** in 55% yield (Table 1S, entry 1). However, two sets of signals were visible on the ^{19}F NMR spectrum indicating the presence of two diastereoisomers and thus the epimerization of at least one Cα. By decreasing the reaction time to 5 hours, no epimerization was visible and **3** was obtained in satisfactory 48% yield (Table 1S, entry 2). We also tried to use a weaker base such as collidine and no epimerization was observed (Table 1S, entry 3). In order to try to increase the yield, we screened other coupling conditions (SI, Table 1S, entries 4–8) but none gave better yields. The Boc cleavage of **3** was conducted to afford compound **4** (97% yield) which was then acetylated to give compound **5** in satisfactory yield (88%). Similar to the procedure followed to obtain **3**, compounds **16** and **19** were submitted to hydrogenolysis and acidic treatment respectively to obtain the free carboxylic acid and amine intermediates, which were coupled to give compound **20** in 42% yield. Its Boc cleavage using the cleavage cocktail TFA/H_2O/TIPS/thioanisole (scavengers were necessary to avoid trityl addition on the triazole rings) gave **6** (61% yield) which was acetylated to give **7** in 50% yield.

To prepare compounds **8** and **9**, we followed a slightly modified procedure reported by us.[55] The synthesis, outlined in Scheme 2, started from scaffold **21** that was prepared in accordance with our published procedure[69,70] Contrary to what we reported for the coupling of a simple tripeptide or a di-aza-tripeptide on the carboxylic group of our scaffold moiety,[55,71] here we had to prepare the doubly (Boc and Tosyl) protected scaffold **22** because the acidic proton of the NH-Tosyl led to an undesired and predominant intra-cyclisation during the coupling reaction between the peptidomimetic arms and the carboxylic acid (see Figure 47S, SI,). Thus, a Boc protection of the NH-Tosyl using Boc_2O in the presence of DIPEA and DMAP allowed the double protected intermediate **22** (93% yield). The benzyl group on the piperidine ring was cleaved by hydrogenolysis to give **23** quantitatively. The three successive coupling reactions using the amino acids *N*-Fmoc-L–Leu–OH, *N*-Fmoc–L–Ile–OH, and *N*-Boc-L–Ala–OH, followed by the basic

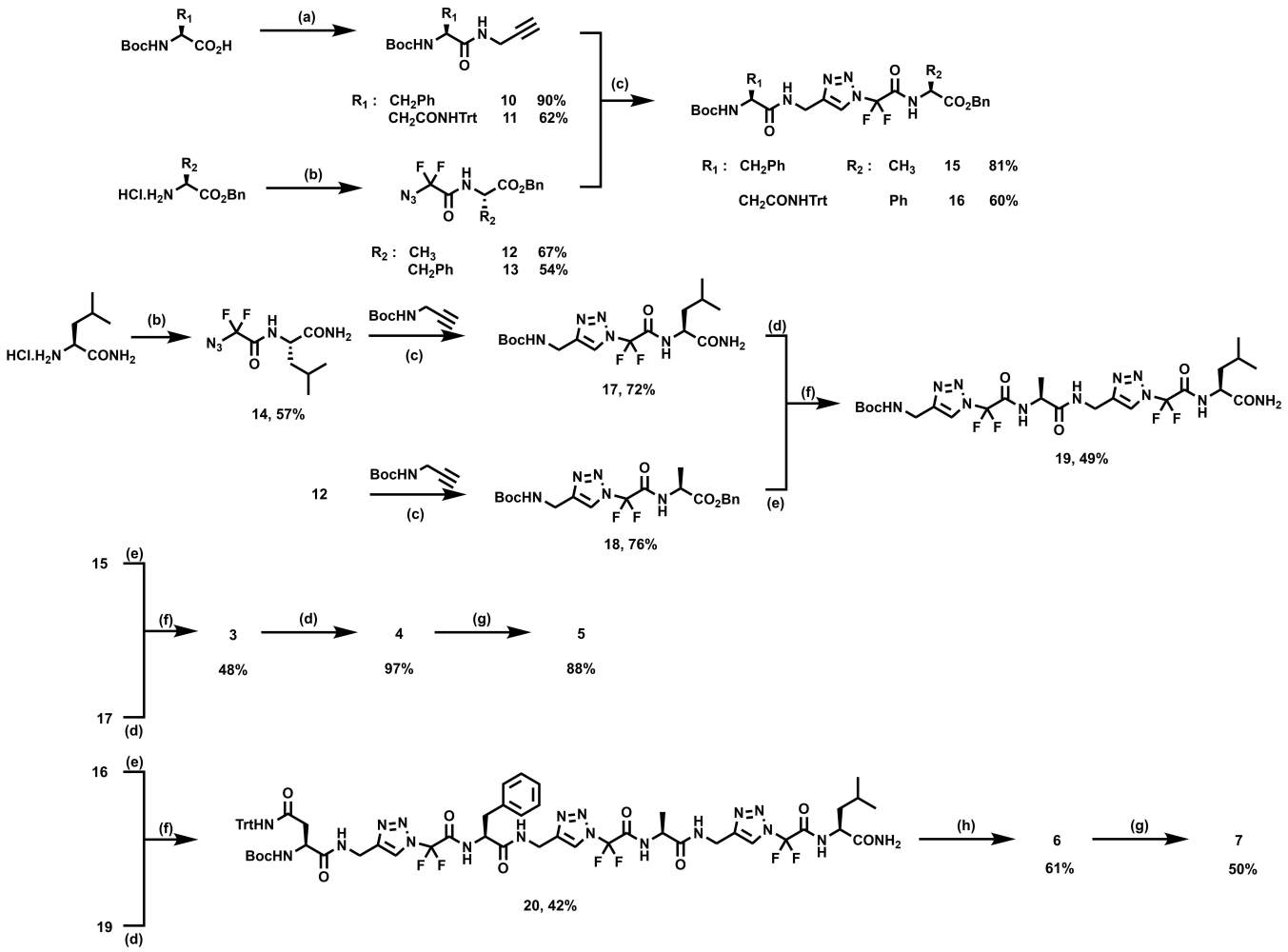

Scheme 1. Synthesis of compounds **3**–**7**. (a) propargylamine (1.1 eq.), HOBt (1.1 eq.), EDC.HCl (1.1 eq.), DIPEA (2.5 equiv.), CH_2Cl_2, rt, 5 h; (b) ethyl 2-azido-2,2-difluoroacetate (1 eq.), Et_3N (1 eq.), 4 h,ultrasound; (c) $CuSO_4.5H_2O$ (5%), Asc.Na (20%), TBTA (5%), MeOH/H_2O, rt, 2 h; (d) HCl 4 N in dioxane (10 eq.), CH_2Cl_2; or CH_3OH, rt, 1 h (e) Pd/C (30%), Et_3SiH (2 eq.), MeOH, rt, 30 mn; (f) EDC.HCl (1.2 eq.), HOBt (1.2 eq.), collidine (5 eq.), DMF, rt, 3–5 h; (g) Ac_2O (1.5 eq.), Et_3N (3 eq.), rt, 5 h. (h) TFA/H_2O/TIPS/thioanisole (90/5/2.5/2.5, v/v/v/v), rt, 2 h.

hydrolysis of the ester group of **26** allowed the formation of the key intermediate **27**. The coupling reagents EDC/HOBt in the presence of collidine in dry DCM allowed the couplings in satisfactory yields (73%, 81%, and 67%, respectively, Scheme 2). The coupling of **27** with the two peptidomimetic arms **28** and **29** (synthesized in good yields by following procedures similar to those used to obtain **15** and **16** described above, see SI) was a little bit more challenging and required the use of COMU/Oxyma as coupling agents, in the presence of collidine in dry DMF. It led to **30** and **31** in low to moderate yields (17% and 44%, respectively). Then, the acidic cleavage of the two Boc moieties of **30** and **31** gave the desired compounds **8** and **9**.

Structural Characterization

Conformational Analysis by NMR

The conformational studies of our foldamers **4**–**9** were performed by NMR in the polar and protic methanol-d3 (CD_3OH). The ^1H, ^{13}C, and ^{19}F chemical shift assignments at low temperatures (278 K for **6**–**9** or 283 K for **4**–**5**) are given in Tables 2S-21S (See SI). In compound **5**, the $^3J_{NH\text{-}H\alpha}$ coupling constant values of 7.9 and 8.0 Hz of Phe-1 and Leu-3 (see Table 4S, SI) correspond to the dihedral angles around 120° associated mostly with peptide segments in an extended conformation,[72] as expected for compounds bearing the *N*-difluoromethyltriazole scaffold.[43] However the $^3J_{NH\text{-}H\alpha}$ of Ala-3 was more difficult to reliably calculate but appeared to be below 7 Hz, indicating a more folded structure in this position. The amide bond NH protons temperature coefficients ($\Delta\delta_{NH}/\Delta T$) were then calculated to analyze the backbone conformational propensities. Small negative temperature coefficients (> -4.5 ppb.K^{-1}) correspond to amide protons involved in hydrogen bonds (intra or intermolecular), whereas higher negative values (< -6 ppb.K^{-1}) indicate solvent interactions. In **5**, $\Delta\delta_{NH}/\Delta T$ was calculated between 283 and 313 K (see Table 5S). These values were between -8 and -9 for amide of natural amino acid residue and around -7 for amide bearing 1,4-Tz–CF_2 scaffold indicating that amide bond NH protons were not engaged in

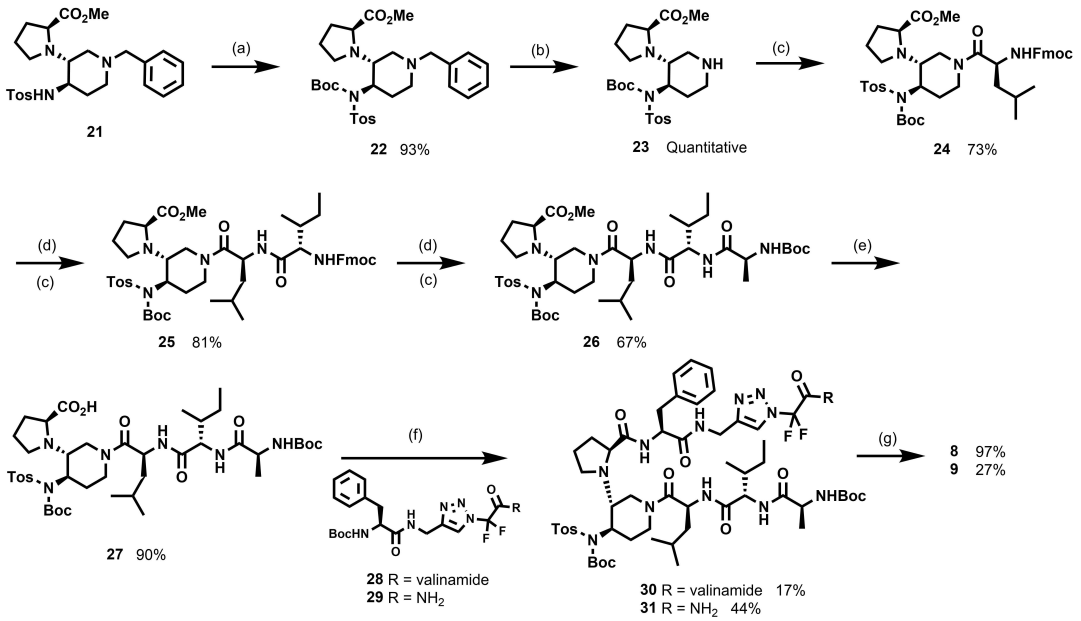

Scheme 2. Synthesis of compounds **8** and **9**. (a) Boc_2O (2.5 eq.), DMAP (2.5 eq.), DIPEA 2.5 eq., DMF, rt, 15 h; (b) Pd/C 10% (1.0 eq.), H_2, 30 °C, 24 h; (c) Fmoc–Leu–OH or Fmoc–Ile–OH or Fmoc–Ala–OH (1.2 eq.), EDC (1.2 eq.), HOBt (1.2 eq.), collidine (2.5 eq.), DCM, rt, 15 h; (d) Piperidine 20% DMF, rt, 4 h; (e) aq. NaOH 2 M (5.0 eq.), MeOH, 40 °C, 3 h then aq. $KHSO_4$; (f) COMU (1.0 eq.), Oxyma (1.0 eq.), collidine (2.5 eq.), DMF, rt, 15 h; (g) HCl 4 N in dioxane (20.0 eq.), DCM, rt, 6 h.

stable hydrogen bonds. Very similar $^3J_{NH\text{-}H\alpha}$ and $\Delta\delta_{NH}/\Delta T$ values were obtained for compound **4** (see Tables 2S and 3S in SI). Long-range ^1H–^1H ROE correlations were observed indicating a folded conformation for heterotriazolamers **4** and **5**. In both **4** and **5**, ROEs were visible between the CH_3 of Ala-3 and the H_c of the two triazoles, TZL-2 and TZL-4. In **5**, correlations between CH_3 of Ala-3 and H_α of Phe-1, and between H_β of Phe-1 and H_c of TZL-2 were also observed (Figure 2). The two amino acids on either side of the TZL-2 unit could be brought together thanks to the flexibility of the C_α of TZL units. In fact, this part of the *N*-difluoromethyltriazole scaffold has a higher flexibility than the part bearing the two fluorine atoms which is responsible for the constraining effect of the scaffold thanks to H–F interactions (Figure 2).[43] In the case of the NH_2-free analogue **4**, one ROE was visible between H_α of Phe-1 and H_c of TZL-2. The direct rapprochement between Phe 1 and Ala-3 was not visible. Very similar NMR data were obtained for the longer heterotriazolamers **6** and **7**. The amide bond NH protons temperature

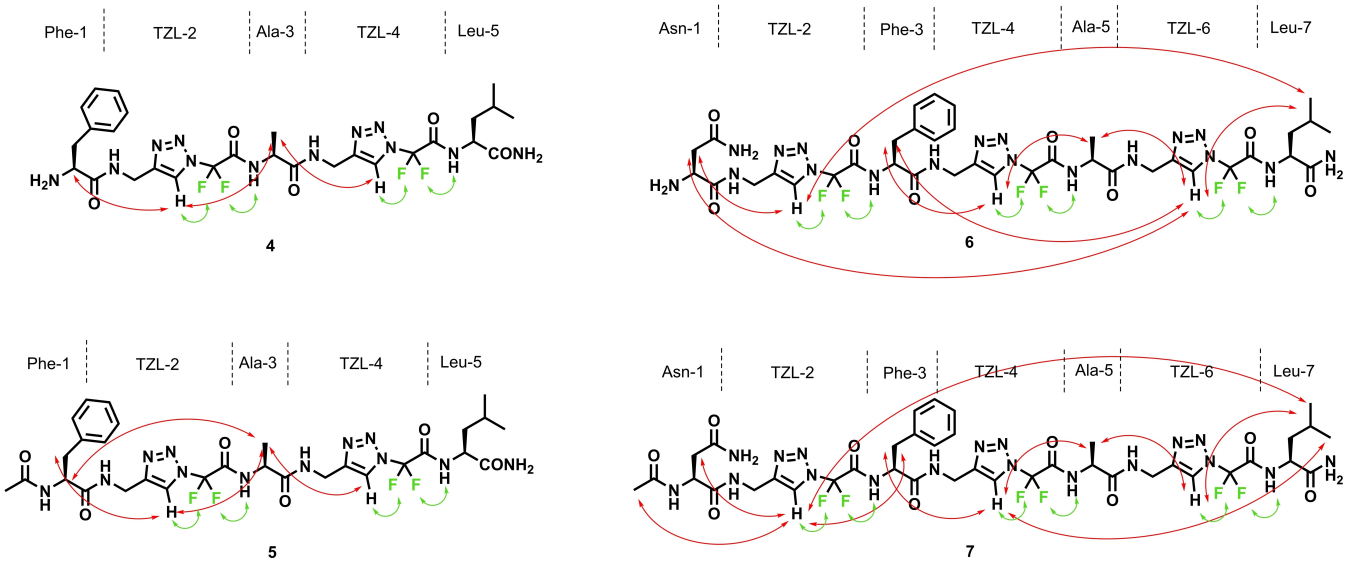

Figure 2. NMR conformational analysis of heterotriazolamers **4**, **5**, **6**, and **7**: long-range ^1H–^1H ROE (red) and ^1H–^{19}F NOE (green) correlations observed in CD_3OH (3 mM) at 283 K (**4**, **5**) and 278 K (**6**, **7**).

coefficients ($\Delta\delta_{NH}/\Delta T$) were all lower than −6 ppb.K^{-1} indicating that they are not involved in H-bonds (see Tables 7S and 9S, SI). Although some $^{3}J_{NH\text{-}H\alpha}$ of **6** and **7** were difficult to determine, the two $^{3}J_{NH\text{-}H\alpha}$ values for TZL-2 and −4 of **6** and **7** were below 7 Hz, indicating the folding around the C_α of TZL units. Many long-range ^{1}H–^{1}H ROE correlations were observed further confirming folded conformations for **6** and **7** (Figure 2). In particular between CH_β of Asn-1 and H_c of TZL-2, CH_β of Phe-3 and H_c of TZL-2 and TZL-4 (only TZL-4 for **6**), CH_3 of Ala-3 and H_c of TZL-4 and TZL-6, and CH_δ of Leu-7 and H_c of TZL-6. A very long-range ^{1}H–^{1}H ROE correlation was also observed between CH_δ of Leu-7 and H_c of TZL-2 in both **6** and **7**, as well as between CH_β of Asn-1 and H_c of TZL-6 in the case of **6**, indicating a close proximity between the N- and C-termini of heterotriazolamers **6** and **7**.

In the 2D ^{19}F–^{1}H HOESY spectra of **4** –**7**, only the short-range correlations involving in each 1,4-Tz–CF_2 unit the two fluorine atoms with the proton of the triazole and the NH of the successive unit were visible (Figures 2 and 9-10S, 17–18S, 24–25S and 31–32S in SI). This result suggests that the two fluorine atoms of each 1,4-Tz–CF_2 unit maintained the extended constraint at its C-terminal part but were not involved in the overall folding of the foldamers.

The conformational behaviour of **8** and **9** was similar to that of our previously reported acyclic β-hairpin like structures bearing the tripeptide arms and the di-aza-tripeptide.[55] They displayed the presence of two major conformers in dynamic equilibrium. The complete assignment of the ^{1}H and ^{13}C signals was performed for the two conformers of compounds **8** and **9**. Working at 278 K allowed the observation of two different conformers in dynamic equilibrium in ratios 3:1 and 1:1 for **8** and **9** respectively. However, in contrast with **9**, despite the low temperature, some protons and carbons displayed the same chemical shift in both conformers of **8**. The ^{1}H-NMR and ^{13}C-NMR chemical shifts are reported in Tables 10S and 11S (SI) respectively for conformers A and B of **8**. In both conformations (Table 12S, SI) only the $^{3}J_{NH\text{-}H\alpha}$ coupling constant for Ile-2 and Val-8 values fell within the range of 8–12 Hz that correspond to the dihedral angles associated with peptide segments in extended conformation as expected for β-hairpin arms.[72] These results suggested that compound **8** was not fully structured. In both conformers, NH-CSD generally showed positive values as expected for the extended arms of a β-hairpin (Tables 13S and 14S, SI). However, the general C-CSDs up-fielding (Table 13S and 14S, SI) of both conformers confirmed the presence of extended conformations of the arms. While the positive C^{α}-CSD of Pro-5 indicated the presence of a β-turn inducer in both conformations. In conformer A, $\Delta\delta_{NH}/\Delta T$ calculated between 278 and 313 K were smaller than −4.5 suggesting no stable H-bond (see Table 15S, SI). In both conformers, the presence of sequential $CH\alpha_i/NH_{i+1}$ ROEs for the tripeptide FLV and for the segment from Pro-5 to Tzl-7 confirmed the extended conformation of the arms (Figure 3, blue arrow). Concerning the ROE network usually observed in the β-turn region for similar compounds,[55] we observed only the ROE between H^{α}-Pro-5 and proton in position 3 of the piperidine ring (Figure 3, green arrow). The two different ROEs displayed by the H^{α}-Leu-3 with the piperidine ring were more interesting. Indeed, in conformer A we observed an ROE signal of H^{α}-Leu-3 with proton in position 2 while in conformer B the ROE was visible between H^{α}-Leu-3 and proton in position 6. As we recently demonstrated,[55] of these signals are diagnostic of two different architectures: one more closed (conformer A) and one more open (conformer B). Furthermore, we observed spatial proximities between the lateral chains of Leu-3 and Phe-6, reflecting the interaction between the two arms, only in the case of conformer A as expected for the more closed patterning. However, the ROE between the CH_2 of Phe-6 with the CH_3 of Val-8 suggested a folding of the peptidomimetic arm around the CF_2–Tz. This is in accordance with the folding observed in the triazolamer **5** indicating a rapprochement between the two amino acids on each side of the TZL-2 unit.

The complete attribution of two conformers A and B of **9** was performed (Tables 16S and 17S respectively for conformers A and B, SI). By analyzing the CSDs for each natural amino acid present in the structures (Tables 18S and 19S, SI), we observed, in both conformers, that the residues Ile-2, Leu-3, and Phe-6 showed a general down-fielding for α hydrogens and amides compatible with an extended conformation, while Ala-1 and Pro-5 displayed negative values indicating flexibility at the *N*-terminal and a β-turn conformation for Pro-5. The negative C-CSDs further confirmed possible extended conformation of the arms, while the very small Cα and carbonyl CSD Pro-5 values confirmed its involvement in a β-turn. The measurable $^{3}J_{NH\text{-}H\alpha}$ displayed large values systematically higher than 8.9 Hz, reflecting extended arms (Table 20S, SI). In conformer A, $\Delta\delta_{NH}$/

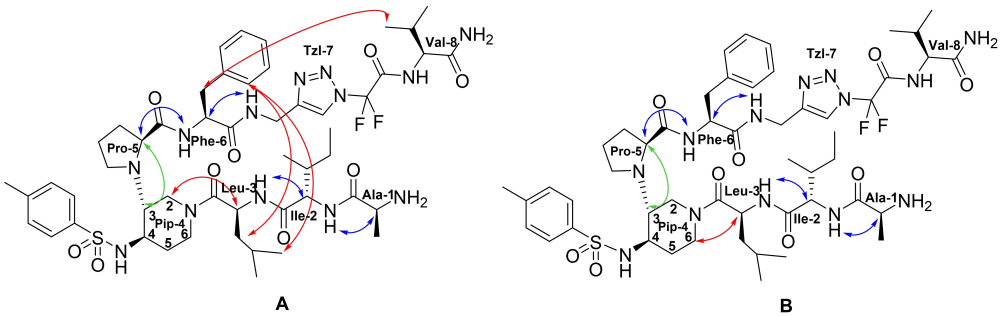

Figure 3. In green are the common ROEs, in blue are the common sequential ROEs, and in red are the differences between conformers A and B of compound **8** observed in CD_3OH at 278 K (3 mM).

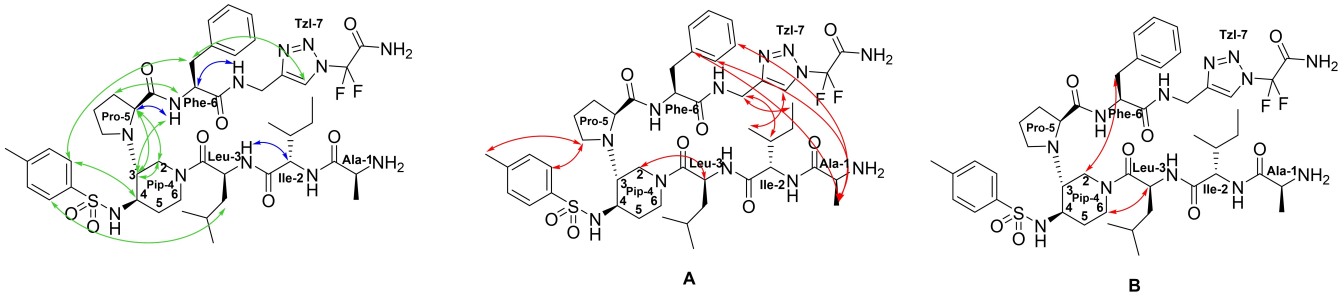

Figure 4. Structure of compound **9** showing the ROE networks. In green are the common ROEs, in blue are the common sequential ROEs, and in red are the differences between conformers A and B observed in CD_3OH at 278 K (3 mM).

ΔT calculated between 278 and 313 K were superior to −4.5 in the case of Phe-6 and Tzl-7 suggesting their involvement in H-bonds (−2.9 and −3.2, respectively, Table 21S, SI). The arms of both conformers showed the characteristic pattern of sequential $CH\alpha_i/NH_{i+1}$ ROEs typical of extended peptides (Figure 4, blue arrow). This sequence was interrupted only for the terminal Ala-1, further confirming the more flexible *N*-terminus. Both conformers had the typical ROE pattern of a β-turn inducer (Figure 4, green arrows[55]). Here again, conformer A presented numerous spatial proximity signals between the upper and the lower arms, unlike conformer B (Figure 4, red arrows). H^{α} Leu-3 had ROE signal with protons in positions 2 and 6, respectively, for conformers A and B of the piperidine ring. Both observations confirmed the presence of a more closed (conformer A) and one more open (conformer B) architecture.

Conformational Analysis by Molecular Dynamics

To gain better insight into their preferential structures, compounds **4** and **5** were each submitted to a 500 ns all-atom molecular dynamics simulation in explicit methanol solvent. The theoretical $^3J_{NH\text{-}H\alpha}$ coupling constants (computed over the whole trajectories) are fairly close to the experimental measurements (Table 1), indicating that the conformational ensembles generated by MD simulations are consistent with those revealed by NMR.

Regarding interproton distances within the two molecules, the NMR observations are partially retrieved in MD simulations.

Table 1. Comparison of $^3J_{NH\text{-}H\alpha}$ coupling constants (Hz) in compounds **4** and **5** measured by NMR or computed by MD simulations in methanol at 300 K.

Residues	Compound **4**		Compound **5**	
	NMR	MD	NMR	MD
Phe 1	–	–	7.4	7.6 ± 1.6
TZL 2	6.3	4.9 ± 2.6	5.9	4.4 ± 2.6
Ala 3	6.8	7.5 ± 1.7	7.3	7.5 ± 1.7
TZL 4	5.6	4.8 ± 2.7	5.8	4.9 ± 2.7
Leu 5	8.8	8.0 ± 1.5	8.0	8.0 ± 1.4

As shown in Figure 5, distances between Phe1 Hα or Hβ protons and H_c of TZL-2, as well as distances between Ala-3 Hβ protons and H_c of both neighbouring TZL-2 and TZL-4, reached values below 0.5 nm in a significant number of conformations, which is consistent with detected NOE. Nevertheless, contrary to NMR experiments of compound **5**, but consistent with those of compound **4**, we did not observe close proximity of Phe-1 Hα (or Hβ) with Ala-3 Hβ in MD simulations. This indicates that the Phe1-TZL2-Ala3 segment is more extended in compound **5** simulation than *in vitro*. A similar extended conformation of the second half Ala3-TZL4-Leu5 segment in both compounds is supported by no detection of long-range NOE between Ala3 and Leu5 protons.

Overall, MD simulations of compounds **4** and **5** generated conformational ensembles in which the two rather rigid extended segments Phe1-TZL2-Ala3 and Ala3-TZL4-Leu5 can rotate around Ala3 residue which act as a hinge, allowing conformational transitions between folded hairpin-like and more extended linear structures (Figure 6).

Since MD simulations of molecules **4** and **5** could generate conformational ensembles in fair agreement with NMR experiments, we used the same method to propose structural models of compounds **6** and **7**. MD trajectory visualizations show that both molecules **6** and **7** are highly flexible and dynamically adopt different conformations As shown in Figure 49S (SI)

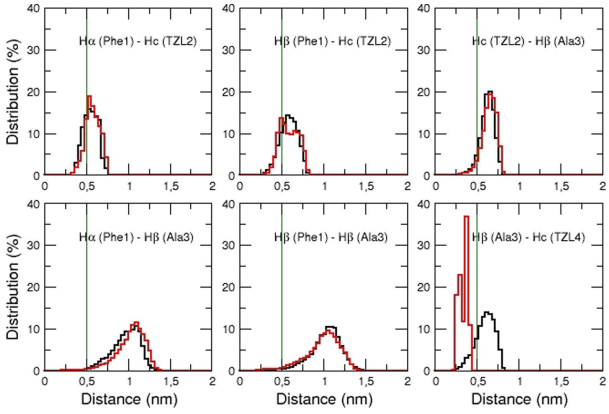

Figure 5. Distribution of interproton distances computed from MD trajectories of compound **4** (black lines) and compound **5** (red lines). Vertical green lines indicate the distance below which NOE can be detected.

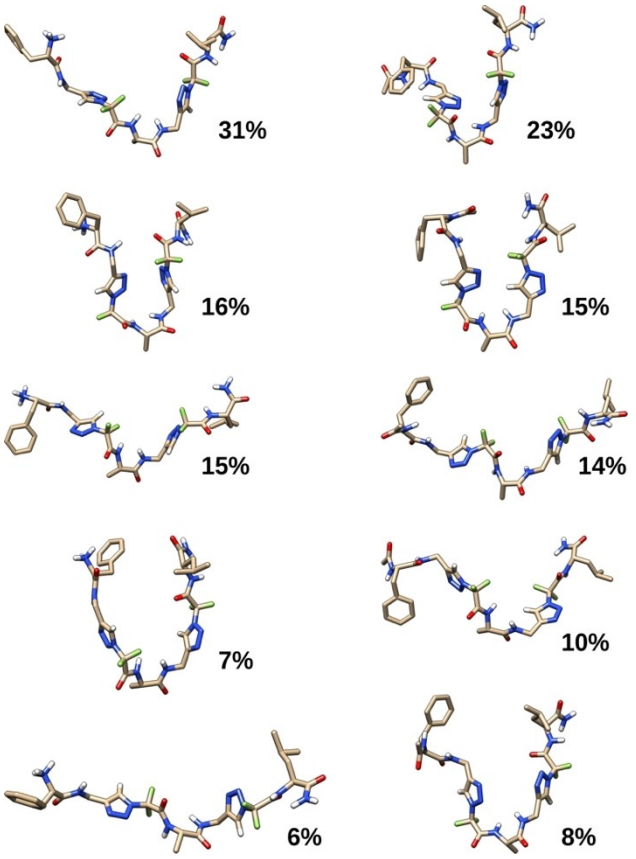

Figure 6. Representative structures of the five most populated clusters of compounds **4** (left column) and **5** (right column). The RMSD threshold for clustering is 0.3 nm.

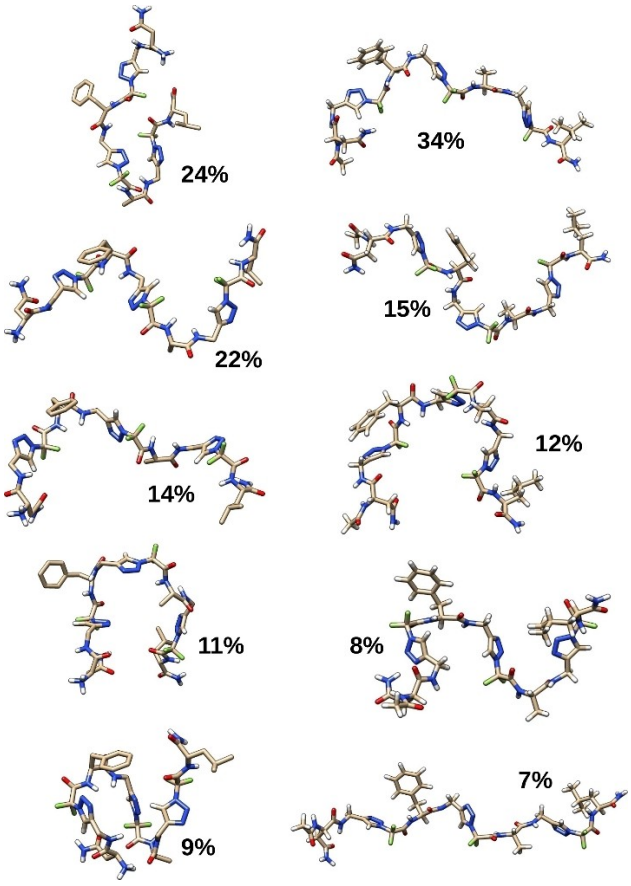

Figure 7. Representative structures of the five most populated clusters of compounds **6** (left column) and **7** (right column). The RMSD threshold for clustering is 0.4 nm.

which displays the distribution of the RMSD values between all pairs of conformations generated for each simulated compound, the bell-shaped curves for compounds **6** and **7** are broader and shifted toward higher values than for compounds **4** and **5**, indicating that the former are more flexible and sample more diverse conformations than the latter. The representative structures of the five most populated clusters of compounds **6** and **7** are displayed in Figure 7. Like in compounds **4** and **5**, we noticed that the 3 Asn-TZL, Phe-TZL, and Ala-TZL fragments are rather rigid, but can rotate around the 2 residues Phe and Ala which act as hinges. Thus, we could observe transient hairpin-like structures or zig-zag conformations bent at these two positions, which sometimes fold into ladder-like structures similar to short multi-stranded β-sheets. It should be noted that the population of these transient folded structures could be underestimated in MD simulations compared to experiments. Indeed, as shown in Figure 48S (SI), the interproton distances between non-adjacent "residues" (Asn1-TZL6, TZL2-Leu7, Phe3-TZL6, and TZL4-Leu7) are most often larger than 0.5 nm in simulations, whereas corresponding long-range ^{1}H–^{1}H ROEs are observed in NMR experiments. This indicates that NMR conformations of compounds **6** and **7** are probably more frequently folded (or structured) than those generated by simulations. Since inhibition assays of these compounds are performed in water, unlike NMR experiments which were done in methanol, we additionally ran MD simulations of compounds **5** and **7** in explicit water and compared the water versus methanol conformational ensembles. As indicated by the RMSD distributions of Figure 49S (SI), both compounds **5** and **7** were slightly more flexible and sampled more diverse conformations than in methanol. Nevertheless, the transient hairpin-like structures of compound **5** are still significantly retrieved in water as in methanol (Figure 50S, SI). It could also be noted that conformations of compound **7** appear slightly more compact but less structured in water than in methanol.

Activity on hIAPP Fibrillization by ThT-Fluorescence Experiments

The ability of foldamers **1**–**9** to interact with hIAPP fibril formation was first investigated using the *in vitro* Thioflavin-T (ThT) fluorescence assay (representative curves are shown in Figures 8 and 52S, SI). Heterotriazolamers **3**–**5** and **6**–**7** were compared to the natural peptides FGAIL-NH_2 and NNFGAIL-NH_2, respectively, and the homotriazolamers **1** and **2**. Flexible β-hairpin like structures **8** and **9** were compared to their peptide analogues bearing AIL and FLV arms and reported as inhibitors of hIAPP aggregation.[55] ThT is the standard dye used to monitor the kinetics of aggregation of amyloid proteins

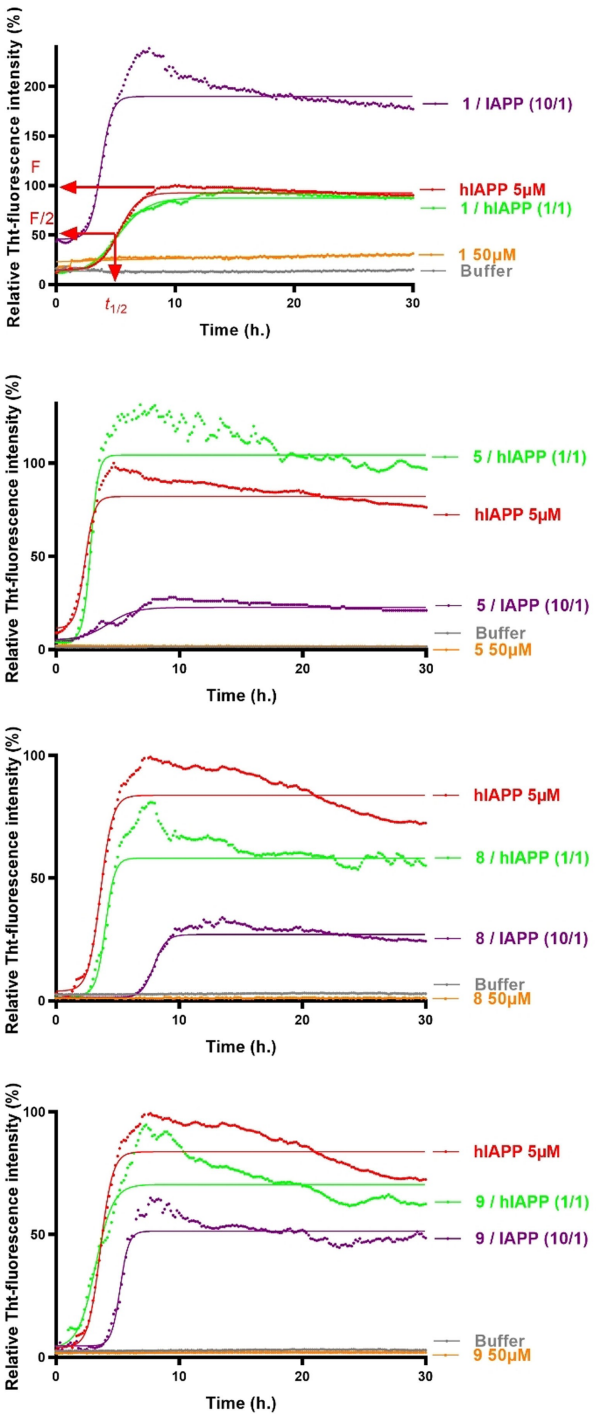

Figure 8. Representative curves of ThT fluorescence of one assay over time showing hIAPP control aggregation (5 µM) in the absence (red curve) and in the presence of compounds **1**, **5**, **8**, and **9** at compound/hIAPP ratios of 10/1 (purple curves) and 1/1 (green curves). The control curves are represented in orange lines and the buffer in grey. Solid lines correspond to curves fitted with a Boltzmann sigmoidal model.

because it fluoresces upon binding to β-sheet rich structures.[73,74] The fluorescence curves for hIAPP controls displayed the typical sigmoidal pattern, starting with an initial lag phase lasting around 1 h, followed by a rapid polymerization phase ending with a plateau reached after 5 h. Two parameters were gathered from the fluorescence curves analysis: (1) $t_{1/2}$, defined as the time at which fluorescence has reached half of its maximal value and gives insight into the kinetics of the aggregation process, and (2) F, the fluorescence intensity at the plateau, which is, in a first approximation, related to the amount of fibrillar material formed. Each compound was tested at two different foldamer/amyloid peptide ratios, 10/1 and 1/1, and variations of $t_{1/2}$ and F are reported in Table 2.

The aggregation curves of hIAPP in the presence of homotriazolamer **1** at **1**/hIAPP ratio 10/1 (Figure 8) showed a shorter $t_{1/2}$ and a higher fluorescence plateau than for the control experiment indicating that compound **1** is capable of accelerating but also increasing the aggregation of hIAPP. These observations were not found at the lower ratio of 1/1. This higher fluorescence plateau could be due to a slight self-association of **1** (seen in Figure 8, orange curve) which can seed and thus trigger the aggregation process of hIAPP. However, this phenomenon is not associated with insolubility of **1** (as

Table 2. Table summarizing the effects of compounds **1**–**9**, FGAIL-NH_2, and NNFGAIL-NH_2 on hIAPP fibrillization assessed by ThT-fluorescence spectroscopy at 10/1 and 1/1 ratios of compound/hIAPP.

Compound	Compound/ hIAPP ratio[a]	$t_{1/2}$ extension/ reduction (%)[b]	F extension/ reduction (%)[c]
1	(10/1) [d]	−30±8%	+94±37%
	(1/1)	ne	ne
2	(10/1)[d]	ne[e]	−24±15%
	(1/1)	ne	ne
3	(10/1)	−42±12%	−49±4%
	(1/1)	+15±9%	−41±9%
4	(10/1)	ne	ne
	(1/1)	ne	ne
5	(10/1)	+112±42%	−80±8%
	(1/1)	+15±7%	ne
6	(10/1)	+42±25%	ne
	(1/1)	ne	−33±15%
7	(10/1)	ne	ne
	(1/1)	ne	ne
8	(10/1)	+106±32%	−64±5%
	(1/1)	ne	−28±13%
9	(10/1)	+46±18%	−37±9%
	(1/1)	ne	ne
FGAIL-NH_2	(10/1)	ne	−36±3%
	(1/1)	ne	ne
NNFGAIL-NH_2	(10/1)	+14±8%	−14±10%
	(1/1)	ne	−24±13%

Parameters are expressed as mean±SE, n=3 of one triplicate assay.[a] Compounds were dissolved in DMSO; the final concentration was kept constant at 3% (v). The concentration of hIAPP was 5 µM.[b] See supporting information for the calculation of the $t_{1/2}$ extension/reduction.[c] See supporting information for the calculation of the F extension/reduction.[d] Compounds **1** and **2** are slightly self-associate at 50 µM.[e] ne=no effect: extension/reduction equal to zero.

demonstrated by UV measurement see SI, Figure 53S). The longer homotriazolamer **2** displayed no effect on the aggregation process of hIAPP while its slight self-aggregation was also observed at 50 μM (Figure 52S).

Concerning the heterotriazolamers built on the FGAIL sequence, surprisingly, the Boc-protected analogue **3** displayed a slight acceleration of the fibrillization kinetics associated with a decrease of the plateau at 10/1 ratio ($\Delta t_{1/2} = -42\%$, $\Delta F = -49\%$; Table 2 and Figure 52S, SI); with only the effect on the fluorescence plateau being maintained at the lower ratio 1/1. However, the *N*-terminal free amine analogue, compound **4**, was found to be inactive regardless of the ratio tested (Table 2 and Figure 52S, SI). In this series, compound **5**, acetylated at the *N*-terminal part, showed the most interesting effect, stronger than the peptide analogue FGAIL, with a pronounced activity at **5**/hIAPP ratio 10/1 (Figure 8), both on the fibrillization kinetics ($\Delta t_{1/2} = +112\%$ for **5** vs no effect for FGAIL-NH_2) and on the fluorescence plateau ($\Delta F = -80\%$ for **5** vs $= -36\%$ for FGAIL-NH_2). The activity was not retained at the lower ratio of 1/1.

The longer heterotriazolamers **6** and **7** designed on the NNFGAIL sequence, displayed weaker activity than the FGAIL built analogues (Table 2 and Figure 52S, SI). The *N*-terminal free amine **6** slightly delayed the aggregation process at a 10-fold excess ($\Delta t_{1/2} = +42\%$) and showed no effect on the fluorescence plateau, while at 1/1 ratio, it displayed no effect on the kinetics and a modest decrease of the fibrillization plateau ($\Delta F = -33\%$). Unlike in the FGAIL-based series, the acetyl analogue **7** based on the NNFGAIL series was inactive at all ratios tested, which seemed consistent since its peptide parent NNFGAIL-NH_2 is reported in the literature as the shortest hIAPP sequence forming fibers of identical morphology as the 37 isoform peptide.[62]

The flexible β-hairpin like **8** bearing an AIL peptide at the *N*-terminus and an F-(1,4-Tz–CF_2)–V arm at the *C*-terminus significantly delayed the fibrillization kinetics ($\Delta t_{1/2} = +106\%$) and decreased the fibrillization process ($\Delta F = -64\%$) at ratio 10/1 as seen in Figure 8 and Table 2. At the lower ratio of 1/1, the activity was weaker with only a modest reduction of the fluorescence plateau ($\Delta F = -28\%$) and no effect on the kinetics. In comparison, the shorter analogue **9** bearing an F-(1,4-Tz–CF_2) arm at the *C*-terminus retained the activity but to a lesser extent, being half active as the longer analogue **8** ($\Delta t_{1/2} = +46\%$ and $\Delta F = -37\%$ at **9**/hIAPP 10/1 ratio). No noticeable effects were observed at the lower ratio. Overall, this activity was observed only at a 10:1 ratio while the peptide analogue was still active at the lower ratios 1:1 and 0.1:1.[55]

Thus, among the nine evaluated compounds, homotriazolamer **1** and heterotriazolamer **5** showed a higher ability to interact with hIAPP at a compound/hIAPP 10/1 ratio. However, while **1** adopting an extended conformation dramatically increased the fibrillization process, on the contrary, the folded heterotriazolamer **5** decreased it. Furthermore, **5** is more active than its natural parent FGAIL-NH_2.

Effect on hIAPP Oligomerization by Native and Ion Mobility Mass Spectrometry Experiments

Mass spectrometry (MS) has been used as a valuable technique to identify oligomeric species formed during the early oligomerization process of amyloid peptides and proteins.[75] It represents a complementary method to the ThT-fluorescence assay which focuses more on the subsequent formation of fibrils. Moreover, it is a powerful tool to study the mechanism of hIAPP aggregation modulators.[76–81] In order to have information on the effect of these series of foldamers on the oligomerization process of hIAPP, native mass spectrometry (MS) experiments, using our reported method,[76,29,55] were carried out at different incubation times (from T0h to T2h, corresponding to the period when monomers and small oligomers are visible and allowing to follow the effect of compounds). Three foldamers, displaying different ThT-fluorescence behaviours, were selected and tested: the homotriazolamer **1**, accelerating hIAPP fibrillization, the FGAIL-built heterotriazolamer **5**, demonstrating a delaying effect and the longer NNFGAIL-based heterotriazolamer **7**, being inactive on hIAPP fibrillization. Compounds were tested at 3 different foldamers/hIAPP ratios: 10/1, 5/1, and 1/1. As their effects were similar at the 2 higher ratios and showed no effect at the lowest ratio, we will only discuss the 5/1 ratio (Figure 9).

As already reported, the MS spectrum of hIAPP alone at T0 showed a common set of multicharged monomeric and oligomeric species; from dimers to hexamers that decreased progressively, and at T2h, only monomers to trimers were still visible (Figure 9a).

In the presence of homotriazolamer **1** at T0h, only hIAPP monomeric, dimeric, and trimeric species were detected (M, 2 M, and 3 M), the larger oligomers being indetectable (Figure 9b). The spectrum was similar at T2h concerning these species. Noticeably, non-covalent complexes of **1** with hIAPP monomers and dimers ([M + **1**], [M + 2.**1**], [M + 3.**1**], [2 M + **1**] and [2 M + 2.**1**]) were seen at T0 but become indiscernible at T2h. Some clusters of **1** were also detected, from [2.**1**] to [4.**1**], indicating self-aggregation of **1** or specific associations maybe due to its relatively high concentration (Figure 9b).

In the presence of heterotriazolamer **5** (Figure 9c), at T0h, only hIAPP monomers and (M) dimer (2 M) were detected while larger oligomers, trimers to hexamers, were invisible. Moreover, 14 non-covalent complexes of **5** with almost exclusively hIAPP monomers were seen (from [M + **5**] to [M + 10.**5**]) at T0 and some were stable at T2h, indicating a strong interaction between heterotriazolamer **5** and hIAPP monomer. Like for **1**, some clusters of **5**, from [2.**5**] to [9.**5**], were also detected only at the initial time of the kinetics.

In the presence of the longer heterotriazolamer **7**, at T0h only monomeric species of hIAPP were detectable (M) with an intensity significantly weaker than for the control experiment (Figure 9d). Non-covalent complexes of **7** with hIAPP monomeric forms were seen ([M + **7**] to [M + 5.**7**]) at T0h and some of them were stable at T2h ([M + **7**] and [2 M + **7**]).

Then, we performed some ion mobility experiments that allowed the separation of conformers according to their shape,

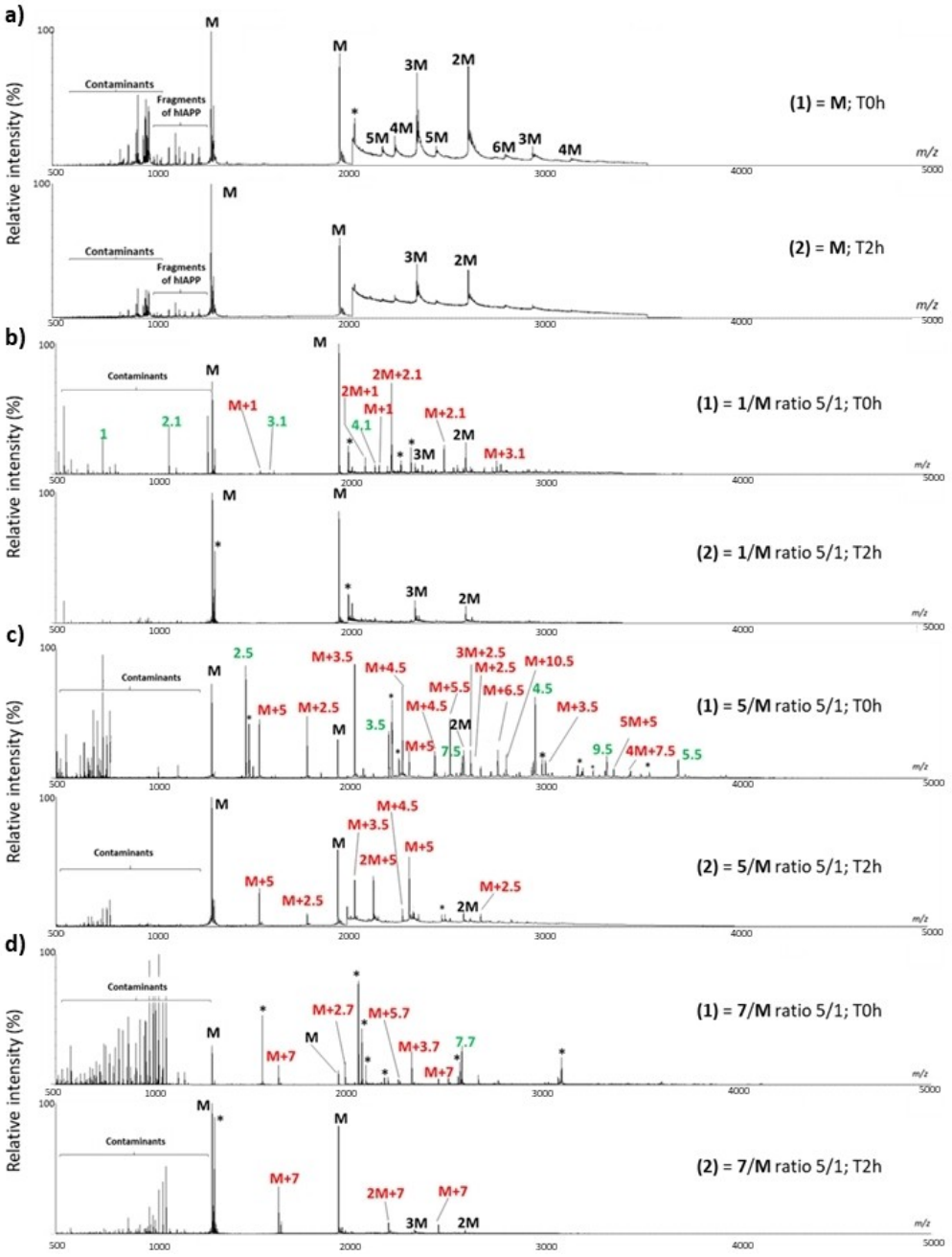

Figure 9. a) Mass spectra recorded in native electrospray ionisation for the 500–5000 range of hIAPP peptide control at T0h (hIAPP monomer is labeled in bold black as **M** and hIAPP oligomers as **2 M**, **3 M** for the respective dimer, trimer…) **(1)** and at T2h **(2)**; b), c) and d): Mass spectra for the 500–5000 range of hIAPP in the presence of triazolamers **1**, **5** and **7** at T0h **(1)** and T2h **(2)**. The different species are labeled with the number of hIAPP monomers and with the addition of n molecules of dedicated triazolamer corresponding to this complex (e.g. 2 M + 2.**1** in bold red) and the clusters of triazolamers are labeled in bold green. Peaks labeled with an asterisk belong to contaminants. For clarity reasons, the charge states of ions are not mentioned.

charge, and collisional cross section, in order to both describe the qualitative and quantitative conformational profile of specific ions belonging to hIAPP and foldamer complexes between T0 and T2h.[77,78] hIAPP control charges states monomer did not exhibit any change in both qualitative and quantitative conformational landscape from T0h to T2h (Figure 54Sa) and b), SI). In contrast, some ions belonging to hIAPP and **5** complexes like M + **5** and M + 2.**5** exhibited changes in conformer abundances with the stabilization of more compact conformers between T0h and T2h (Figure 54S c), SI). Ion mobility data could not be compared for **1** since all hIAPP + **1** complexes disappeared at T2h. Finally, for **7**, which displayed no effect on fibrilization, no change in conformer abundances between T0h and T2h was observed. Overall, these MS experiments revealed differences between the three foldamers **1**, **5**, and **7** in particular regarding the nature, number, and shape of non-covalent complexes of foldamers with hIAPP monomers/oligomers formed. Foldamer **1**, a fiber formation accelerator in

the ThT experiments, interacts slightly with the monomer while these non-covalent complexes as well as hIAPP oligomers disappear very quickly. Compound **7**, being inactive in the fibrillization process, also interacts with monomeric species to form non-covalent complexes which also disappear fairly quickly, and do not affect the shape and abundance of conformers. On the contrary, foldamer **5**, which significantly delays the fibrillization process in ThT assays, forms numerous non-covalent complexes almost exclusively with hIAPP monomer, which are more compact and stable over time. Thus, it can be hypothesized that foldamer **5** interacts more strongly with the hIAPP monomer, producing its sequestration and favoring a compact conformer that may not be the one prone to aggregation, which could explain the fibrillization delaying effect of **5**.[78]

Interaction with hIAPP by NMR

Proton fluorine-19 NMR Experiments Reveal Compounds 1 and 5 Interaction with hIAPP

The effect of compounds **1** and **5** on hIAPP was first studied using proton NMR experiments and the spectra are shown in Figure 10a. To evaluate the aggregation of hIAPP in the absence and in the presence of compounds **1** and **5**, resonances from amide (N–H) and aromatic protons were analyzed. It should be noted that the amide proton resonances are, in particular, sensitive to the size of the aggregates and often not visible for large-aggregates and fibers. At 0.5 hours, 50 μM of hIAPP (black curve) presented a high-resolution proton NMR spectrum with signals from amide and aromatic protons well resolved. NMR spectra of 250 μM of **1** and **5** compounds in the absence of hIAPP showed a few strong signals that overlap with amide-N–^{1}H signals from hIAPP amide protons. Therefore, for a comparative analysis of the effect of compounds **1** and **5** on hIAPP, a few non-overlapping amide and aromatic signals in the region between the dotted (vertical) lines were considered (Figure 10a). At 0.5 hours, a line-broadening was observed in the presence of **1** or **5** compounds, which could be due to compounds **1** or **5** interacting with monomeric hIAPP or hIAPP aggregation (Figure 55S, SI).

The interaction of compounds **1**/**5** with hIAPP was next probed using ^{19}F NMR experiments. The ^{19}F NMR spectra of the compounds without hIAPP are shown at the bottom of Figure 10b. For achiral homotriazolamer **1** bearing three CF_2 groups, the ^{19}F NMR signals are 3 very close singlets around −88 ppm,[44] while for the chiral heterotriazolamer **5** displaying two CF_2 motifs, the ^{19}F NMR signals are 4 doublets indicating the diastereotopicity of the CF_2 groups in the molecule. An additional ^{19}F NMR signal appeared when mixed with hIAPP at ~−75.6 ppm, ~−75.4 which could be arising from the residual HFIP in the sample. Importantly, a change in signal intensities was observed at ~88 ppm when **1** was mixed with 50 μM hIAPP, as shown in green when compared to the spectrum of the compound alone (Figure 10b, Figure 56S, SI). Similar to **1**, when hIAPP was mixed with **5**, a ^{19}F signal intensity loss of ~40% was

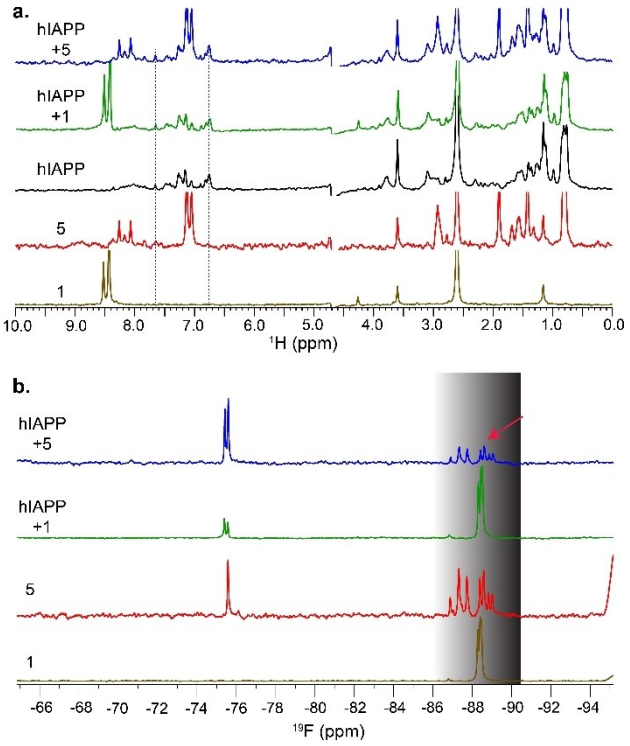

Figure 10. Proton (a) and fluorine-19 (b) NMR spectra of 50 μM hIAPP in the presence and absence of 5 molar excess compounds (**1** and **5**) as indicated, and the reference spectra of 250 μM compounds (**1** and **5**). The proton NMR spectra of hIAPP mixed with compounds shown in green and blue were recorded after ~1 hour of sample preparation. The highlighted region in the ^{19}F NMR spectra indicates a substantial ^{19}F signal broadening in compound **5** mixed with hIAPP as compared to compound **1**. An enlarged spectrum for proton highlighting the region of interest is shown in Supplementary figure 55S.

observed for the peaks in the region ~86–88 ppm relative to **5** in the absence of hIAPP (Figure 10b, blue and Figure 56S, SI).

The measured differences in signal intensities may be attributed to the presence of two different compound populations, hIAPP-bound and hIAPP-unbound, in the mixture containing 5 molar excess of **1** or **5**.

DOSY NMR Experiments Reveal an Increase in the Species Size

The size of species present in samples of compounds **1** and **5** incubated for ~1 hour with and without hIAPP was next determined by measuring the diffusion rate constants using diffusion ordered NMR spectroscopy (DOSY). As shown in Figure 57Sb (SI), the diffusion rate constants measured for **1** in the absence of hIAPP are ~3.9×10^{-10} m^2/s for signals near ~8.45 ppm. On the other hand, incubation of **1** with hIAPP showed a slightly slow diffusion rate constant of ~4.2×10^{-10} m^2/s for the signals at ~8.45 (green signals), respectively, indicating an increase in particle size (Figure 57Sa, SI). Similarly, **5** in the presence of hIAPP (blue signals) showed a slow diffusion rate constant suggesting its complexation with hIAPP. The same diffusion rates (~4.5×10^{-10} m^2/s) measured for the two proton

signals ~7.0 to 7.1 ppm region in the absence of hIAPP, were found to be different in the presence of hIAPP. Further, the time-evolved NMR measurements showed a significant loss of amide proton signals after ~24 hours of sample incubation at room temperature (Figure 57Sa, SI) in the absence of compounds as reported elsewhere[82] and also in the presence of compound **1**, which correlate to our ThT fluorescence observation.

2D SOFAST-HMQC Experiments Reveal hIAPP Aggregation Promoted by Compound 1 and Interaction of 5 with the N-Terminal and Central Parts of hIAPP

To determine the compound's **1**/**5** binding sites in hIAPP, we probed the interaction between **1**/**5** with hIAPP using 2D heteronuclear $^{1}H/^{15}N$ SOFAST-HMQC NMR spectroscopy. A decrease in signal intensity and chemical shift perturbation was observed in the presence of compounds **1**/**5** as seen in the spectra (Figure 11a) and as summarized in plots (b and c). 70 μM of uniformly ^{15}N-labelled hIAPP in the presence of 5 molar excess of **1** or **5** presented a substantial loss in signals for most of the residues in hIAPP: ~40% loss for **1** (Figure 11b, green) and ~20% loss for **5** (Figure 11b, blue). The loss of the NMR signal could be attributed to hIAPP aggregation, which correlates to our fluorescence observation that showed faster aggregation kinetics for hIAPP in the presence of **1**. Chemical shift perturbation analysis presented a relatively higher perturbation in the presence of **5** as compared to **1** (Figure 11c). The N-terminal (10 to 17) and central (25 to 28) residues presented CSP above the average CSP in the presence of **5**; on the other hand, in the presence of **1**, above the average CSP value was observed only for Asn21 located in the central region of hIAPP (Figure 11c).

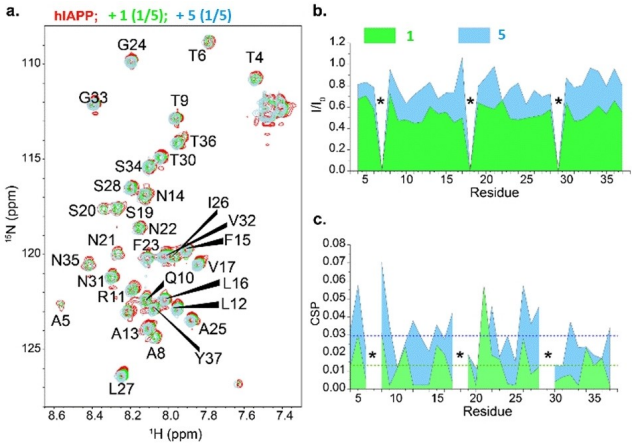

Figure 11. a. 2D SOFAST-HMQC spectra of 70 μM uniformly-^{15}N-labelled hIAPP in the absence (red) and presence of 5 molar excess of **1** (green) and **5** (blue) in 30 mM d3-sodium acetate buffer, pH 5.5 containing 87.5% H_2O, 10% D_2O and 2.5% DMSO-d_6. The resonance assignment was adopted from a previous study.[12] b. Relative change in intensities measured from 2D SOFAST-HMQC spectra (a); where I_0 and I are the signal intensities for hIAPP and hIAPP + triazolamers, respectively. c. Observed chemical shift perturbation (CSP) for hIAPP residues in the presence of **1** (green) and **5** (blue). The average (NH) CSP was calculated using the formula $CSP = \sqrt{\{(\omega_{HN}\Delta^{1}HN)^2 + (\omega_N\Delta^{15}N)^2\}}$, where $\omega_H = 1$ and $\omega_N = 0.154$. The asterisks in (b) and (c) represent unassigned residues of hIAPP.

Conclusions

We described the conformational preferences and activity on hIAPP amyloid protein aggregation of novel fluorinated foldamers based on aminomethyl-1,4-triazolyl-difluoroacetic acid (1,4-Tz–CF_2) units. We demonstrated by NMR experiments and MD simulations that while homotriazolamers of 1,4-Tz–CF_2 unit (**1** and **2**) preferentially adopt an extended conformation,[44] heterotriazolamers (**4**–**7**) showed a significant tendency to adopt transient folded hairpin-like conformations and sometimes ladder-like structures similar to short multi-stranded β-sheets in the case of the longer compounds **6** and **7**. The electrostatic interactions of the two fluorine atoms with the neighbouring triazole CH and the NH of the successive amino acid unit maintain the extended constraint at the C-terminal part of each 1,4-Tz–CF_2 unit. However, the fluorine atoms are not involved in the overall folding of heterotriazolamers **4**–**7** which is due to a kink at the natural amino acid between two triazole units. We hypothesize that π-stacking and/or dipole-dipole interactions between triazole rings induce intermolecular interactions between the less flexible and extended homotriazolamers promoting their aggregation. In contrast, these triazole-triazole interactions are predominantly intramolecular in the more flexible heterotriazolamers which favor their folding and induce hairpin-like and ladder-like structures when two triazoles (**4** and **5**) or three triazoles units (compounds **6** and **7**) are present.

Very interestingly, these three different conformational behaviours seem to dramatically influence the ability of the foldamers to interact with hIAPP and thus their activity on hIAPP aggregation. While extended homotriazolamer **1** accelerates and enhances the aggregation of hIAPP, flexible heterotriazolamer **5** decreases it and the more folded heterotriazolamer **7** has no effect, as shown in thioflavin-T fluorescence assays. The activity of **5** was dramatically increased compared to those of the natural peptide parent FGAIL. *N*-terminal acetylation of **5** is favourable for the inhibitory activity on hIAPP aggregation, as the free amine **4** or the *N*-Boc protected intermediate **3** did not show any interesting activity. ^{1}H and ^{19}F NMR studies confirmed interactions of **1** and **5** with hIAPP. In particular, for **5**, interactions with sequences directly involved in the hIAPP aggregation process (residues 10–17 and 25–28) were observed.[56] Mass spectrometry experiments demonstrated that foldamer **5** interacts with the hIAPP monomer to trap it into a compact conformation delaying its aggregation.

This study highlights the potential of fluorinated peptidomimetic foldamers which were previously unknown as potential modulators of amyloid aggregation or even more widely in the vast field of medicinal chemistry. This work also confirms the interest in fluorine "labeling" for studying by ^{19}F-NMR spectroscopy biological events such as ligand-biomolecule interaction

structure and opens the perspective to use fluorinated foldamers for ^{19}F MRI medical imaging.[83,84]

Experimental Section

Synthesis of Foldamers

The protocols of synthesis of the intermediates **10**, **12**–**14**, **21**–**31** are given in Supporting Information.

General Procedure A: Procedure for the Synthesis of Boc-Protected Aminoacid Propargylamide

To a solution of *N*-(*tert*-Butoxycarbonyl)-L-aminoacid (1.0 eq.) in CH_2Cl_2 (0.38 M) was added propargylamine (1.1 eq.), HOBt (1.1 eq.) and EDC (1.1 eq.). DIPEA (2.5 eq.) was added at 0 °C and then the mixture was let to stir at room temperature for 5 hours. After completion, the solution was diluted with water and extracted with EtOAc. The combined organic layers were successively washed with a 10% aqueous solution of citric acid, and a 10% aqueous solution of K_2CO_3, H_2O, and brine, dried over Na_2SO_4, filtered, and concentrated under vacuum. The crude product was used in the next step without further purification.

General Procedure B: Procedure for Difluorinated Azides Bearing Amino Acid Residues

To a solution of bromodifluoroethylacetate (1.0 eq.) in DMF (0.5 M) was added NaN_3 (1.15 eq.) and the mixture was stirred at 35 °C overnight. After completion (monitored by ^{19}F NMR) triethylamine (1 eq.) and suitable aminoacid (1 eq.) were immediately added and then the mixture was heated in an ultrasound bath for 4 h. The solution was diluted with water (10 mL) and extracted with Et_2O (2×10 mL). The organic layers were successively washed with H_2O (10 mL) and brine (10 mL), dried over Na_2SO_4, filtered, and concentrated under vacuum. The crude product was purified by column chromatography using the appropriate solvents.

General Procedure C: Procedure for the Huisgen Click Reaction for 1,4-Tz-CF_2 Based Oligomers

To a solution of corresponding **azidodifluoroacetylated aminoacid** (1.0 eq.) and Boc-protected propargylamide or propargylamine (1.0 eq.) in MeOH (0.124 M) were successively added $CuSO_4.5H_2O$ (5%), Asc. Na (20%), and TBTA (5%). The mixture was stirred for 2 to 4 hours at room temperature. After completion, monitored by TLC, the solution was diluted in water and extracted with EtOAc. The combined organic layers were successively washed with water and brine, dried over Na_2SO_4, filtered, and concentrated under a vacuum. The crude product was purified by column chromatography using the appropriate solvents.

General Procedure D: General Procedure for the Coupling Step

First, benzyl esters (**15**, **16**, **18**) were deprotected using triethylsilane (2 eq.) and palladium on carbon 30% (0.3 eq.) in MeOH (0.1 M) for 30 minutes at room temperature. The mixture was filtered on a short pad of celite and concentrated under a vacuum to provide the corresponding free acids. Secondly, Boc-protected *N*-difluoromethyltriazoles (**17**, **18**) were deprotected using a solution of HCl in dioxane (4.0 M, 10 eq.) in dry CH_2Cl_2 (0.1 M) for 1 hour at room temperature. The mixture was concentrated under a vacuum to provide respectively the free amines from **17** and **18** which were used in the next step for the coupling reaction with the free acid from **15**, **16**, and **18** previously obtained. So, to a solution of the corresponding acid (1 eq.) in dry DMF (0.38 M) were successively added HOBt (1.2 eq.) and EDC (1.2 eq.). Then, collidine (5 eq.) and the corresponding amine were added at 0 °C. The mixture was let to stir at room temperature for 3 to 5 hours. After completion, the mixture was diluted with water and extracted with EtOAc. The combined organic layers were successively washed with a 10% aqueous solution of citric acid, and a 10% aqueous solution of K_2CO_3, H_2O, and brine, dried over Na_2SO_4, filtered, and concentrated under vacuum. The crude product was purified by flash chromatography using the appropriate eluant.

BocNH-Phe-[TzlCF$_2$]-Ala-[TzlCF$_2$]-Leu-NH$_2$ Heptapeptide (3)

The product was obtained following the general procedure **D** from benzyl ester **15** (240 mg, 0.40 mmol) and **17** (162 mg, 0.40 mmol) which were both deprotected. The crude product obtained was purified by flash chromatography (CH_2Cl_2/MeOH: 99/1 to 90/10) to obtain **3** (154 mg, 0.19 mmol, 48%) as a white solid.; Rf = 0.2 (CH_2Cl_2/MeOH: 95/5); IR: 3276, 3164, 3113, 2932, 2897, 1611, 1546, 1300, 1234 cm^{-1}; Melting point: 122–124 °C; **^{1}H NMR (400 MHz, CD$_3$OD)**:δ 8.40 (s, 1H), 8.23 (s, 1H), 7.26–7.20 (m, 5H), 4.59–4.58 (m, 6H), 4.30 (t, ^3J = 7.3 Hz, 1H), 3.01 (dd, ^3J = 13.6 Hz, ^2J = 8.1 Hz, 1H), 2.99 (dd, ^3J = 13.6 Hz, ^2J = 8.1 Hz, 1H), 1.81–1.69 (m, 3H), 1.50 (d, ^3J = 7.2 Hz, 3H), 1.39 (s, 9H), 0.99 (d, ^3J = 6.2 Hz, 3H), 0.96 (d, ^3J = 6.2 Hz, 3H); **^{13}C NMR (400 MHz, CD$_3$OD):δ** 174.6, 173.1, 172.3, 158.6 (t, ^2J(C,F) = 30.8 Hz), 158.4 (t, ^2J(C,F) = 30.8 Hz), 146.1, 145.8, 137.0, 129.0, 128.0, 126.4, 121.3, 121.1, 110.5 (t, ^1J(F,F) = 267.1 Hz), 110.3 (t, ^1J(F,F) = 267.0 Hz), 79.3, 56.2, 52.3, 50.1, 40.0, 37.7, 34.3, 34.0, 27.3, 24.6, 22.1, 20.2; **^{19}F NMR (400 MHz, CD$_3$OD)**: δ −87.4 (d, ^2J(F,F) = 205.7 Hz, 1F), −88.0 (d, ^2J(F,F) = 205.7 Hz, 1F), −88.6 (d, ^2J(F,F) = 205.7 Hz, 1F), −89.2 (d, ^2J(F,F) = 205.7 Hz, 1F); **HRMS (ESI-TOF)** *m/z* $C_{33}H_{44}N_{12}O_7NaF_4$ $[M+NH_4]^+$ cal. 819.3290, found 819.3292.

NH$_2$-Phe-[TzlCF$_2$]-Ala-[TzlCF$_2$]-Leu-NH$_2$ Heptapeptide (4)

To a solution of **3** (100 mg, 0.126 mmol,1 eq.) in dry CH_2Cl_2 was added drop by drop a solution of HCl in dioxane (4.0 M, 10 eq.). After 2 hours, the mixture was concentrated under vacuum and the crude hydrochloride salt **4** obtained (90 mg, 0.122 mol, 97%) was purified to get a higher purity by preparative HPLC eluting with H_2O + 0.2% formic acid/CH_3CN (gradient 5 to 80% in 20 min) column Pursuit 5 C18 250*10.0 mm R_f = 0.1 (EtOAc/MeOH: 8/2); IR: 3256, 3104, 3016, 2904, 1675, 1586, 1454, 1224, 1192 cm^{-1}; Melting point: 170–172 °C; **^{19}F NMR** (CD_3OD, 564 MHz): δ −84.8 (d, ^2J(F, F) = 204.4 Hz, 1F), −84.9 (d, ^2J(F, F) = 204.4 Hz, 1F), −85.4 (d, ^2J(F, F) = 204.4 Hz, 1F), −85.7 (d, ^2J(F, F) = 204.4 Hz, 1F); **HRMS (ESI-TOF)** *m/z* $C_{26}H_{38}N_{12}O_5NaF_4$ $[M+Na]^+$ cal. 697.2950, found 697.2922. HPLC purity: Sunfire C18 3.5 μm; H_2O + 0.1% formic acid/ACN, gradient 5–100% in 30 min; Rt = 9.43 min, 94%. ^{1}H and ^{13}C NMR data are given in table 2S, SI. ^{1}H, ^{13}C and ^{19}F spectra are respectively given in figures 4S, 5S and 6S, SI.

AcNH-Phe-[TzlCF$_2$]-Ala-[TzlCF$_2$]-Leu-NH$_2$ Heptapeptide (5)

To a solution of unprotected heptapeptide **4** (50 mg, 0.07 mmol, 1.0 eq.) in dry methanol (0.1 M) was added acetic anhydride (1.5 equiv.) and triethylamine (10 mg, 0.1 mmol.,1.5 eq.). After completion, monitored by TLC, the mixture was concentrated under vacuum and purified by silica column chromatography using CH_2Cl_2/MeOH (9/1) as eluant to provide **5** (44 mg, 0.06 mmol, 88%) as a white solid; Rf = 0.2 (CH_2Cl_2/MeOH: 9/1); IR: 3268, 3123, 3100, 2976, 1611, 1546, 1521, 1412, 1402, 1318, 1211, 1132 cm^{-1}; Melting

point: 138–140 °C; **^{19}F NMR (CD_3OH, 564 MHz):** δ −87.9 (d, ^2J(F, F) = 205.5 Hz, 1F), −88.1 (d, ^2J(F, F) = 205.5 Hz, 1F), −89.0 (d, ^2J(F, F) = 205.5 Hz, 1F), −89.3 (d, ^2J(F, F) = 205.5 Hz, 1F); **HRMS (ESI-TOF)** *m/z* $C_{30}H_{38}N_{12}O_6NaF_4$ $[M+Na]^+$ cal. 761.2958, found 761.2961. HPLC purity: XSelect C18 3.5 μm; H_2O + 0.1 % formic acid/ACN, gradient 5–100 % in 30 min; Rt = 12.17 min, 97 %. ^{1}H and ^{13}C NMR data are given in table 4S, SI. ^{1}H and ^{19}F spectra are respectively given in figures 11S and 12S, SI.

NH_2-Asn-[TzlCF$_2$]-Phe-[TzlCF$_2$]-Ala-[TzlCF$_2$]-Leu-NH_2 Decapeptide (6)

2 mL of a cleavage cocktail composed of TFA/H_2O/TIPS/thioanisole (90/5/2.5/2.5, v/v/v/v) was added to compound **20** (10 mg, 0.009 mmol, 1 eq.). After 2 hours of agitation at room temperature, the mixture was precipitated in Et_2O at 0 °C and purified by preparative HPLC (H_2O + 0.2 % formic acid/CH_3CN 5 to 80 % in 20 min, column Pursuit 5 C18 250*10.0 mm) and the compound **6** was obtained (5.5 mg, 0.0056 mol, 61 %) as a white foam after lyophilization. **^{19}F NMR (564 MHz, CD_3OH)**: δ −87.6 (d, ^2J(F,F) = 205.8 Hz, 1F), −87.7 (d, ^2J(F,F) = 204.7 Hz, 1F), −87.9 (d, ^2J(F,F) = 207.7 Hz, 1F), −88.7 (d, ^2J(F,F) = 205.8 Hz, 1F), −88.9 (d, ^2J(F,F) = 204.7 Hz, 1F), −89.5 (d, ^2J(F,F) = 205.8 Hz, 1F) ; HRMS (ESI-TOF, ion polarity positive): *m/z* $C_{37}H_{47}N_{18}O_8F_6$ $[M+H]^+$ cal. 985.3728, found 985.3747. HPLC purity: XSelect C18 3.5 μm; H_2O + 0.1 % formic acid/ACN, gradient 5–100 % in 20 min; Rt = 5.80 min, 100 %. ^{1}H and ^{13}C NMR data are given in table 6S, SI. ^{1}H, ^{13}C and ^{19}F spectra are respectively given in figures 19S, 20S and 21S, SI.

AcNH-Asn-[TzlCF$_2$]-Phe-[TzlCF$_2$]-Ala-[TzlCF$_2$]-Leu-NH_2 Decapeptide (7)

To a solution of compound **6** (50 mg, 0.051 mmol, 1 eq.) in dry methanol (0.1 M) were added acetic anhydride (7.8 mg, 0.077 mmol, 1.5 eq.) and triethylamine (3 eq.). After completion, monitored by TLC, the mixture was concentrated under vacuum and purified by preparative HPLC (H_2O + 0.2 % formic acid/CH_3CN 5 to 80 % in 20 min, column Pursuit 5 C18 250*10.0 mm) and the compound **7** was obtained (25.9 mg, 0.025 mmol, 50 %) as a white solid. **^{19}F NMR (564 MHz, CD_3OH)**: δ −87.6 (d, ^2J(F,F) = 205.6 Hz, 1F), −87.7 (d, ^2J(F,F) = 204.0 Hz, 1F), −87.7 (d, ^2J(F,F) = 205.6 Hz, 1F), −88.6 (d, ^2J(F,F) = 205.6 Hz, 1F), −89.0 (d, ^2J(F,F) = 204.0 Hz, 1F), −89.3 (d, ^2J(F,F) = 205.6 Hz, 1F); HRMS (ESI-TOF, ion polarity positive): *m/z* $C_{39}H_{49}N_{18}O_9F_6$ $[M+H]^+$ cal. 1027.3834, found 1027.3828. HPLC purity: XBridge C18 3.5 μm; H_2O + 0 : 2 % formic acid/ACN, gradient 5–100 % in 20 min; Rt = 6.81 min, 100 %. ^{1}H and ^{13}C NMR data are given in table 8S, SI. ^{1}H, ^{13}C and ^{19}F spectra are respectively given in figures 26S, 27S and 28S, SI.

Compound (8)

To a solution of **30** (44 mg, 0.034 mmol, 1.0 eq) in CH_2Cl_2 (1 mL) under argon atmosphere, was added HCl 4 M in dioxane (170 μL, 0.68 mmol, 20.0 eq.). The mixture was stirred for 6 h at room temperature and Et_2O was added to the suspension formed. After decantation, the solvent was carefully removed with a Pasteur pipette, and the solid obtained was washed twice with Et_2O, and dried under reduced pressure to afford the hydrochloride salt **8** (38 mg, 0.033 mmol, 97 %) as a white powder. **^{19}F NMR (CD_3OH, 564 MHz)**: 2 major conformers (plus one minor) δ −88.1 and −88.2 (d, ^2J(F, F) = 205.0 Hz, 1F); −88.7 and −88.8 (d, ^2J(F, F) = 213.0 Hz, 1F); IR (neat): υ_{max} 3190, 2963, 1655, 1542, 1454 cm^{-1}; HRMS (ESI-TOF, ion polarity positive): m/z $C_{51}H_{75}F_2N_{13}O_9S$ $[M+H]^+$ cal. 1084.5578, found 1084.5576; HPLC purity: XSelect C18 3.5 μm; H_2O + 0.1 % formic acid/ACN, gradient 5–100 % in 20 min; Rt = 13.07 min, 91 %. ^{1}H and ^{13}C NMR data are given in table 10–11S, SI. ^{1}H and ^{19}F spectra are respectively given in figures 33S and 36S, SI.

Compound (9)

To a solution of **31** (94 mg, 0.079 mmol, 1.0 eq) in dry CH_2Cl_2 (1 mL) was added under argon atmosphere at 0° C HCl 4 M in dioxane (396 μL, 1.58 mmol, 20.0 eq.). The reaction mixture was stirred for 6 h at room temperature and to the suspension formed was added Et_2O. After decantation, the solvent was carefully removed with a Pasteur pipette. The solid compound **9** was obtained in quantitative yield as a white solid and was further purified by preparative HPLC eluting with H_2O + 0.2 % formic acid/CH_3CN (gradient 20 to 80 % in 15 min) on an Xselect column (4.6x150 mm–5 μm) to afford the compound **9** (22 mg, 0.021 mmol, 27 %) as a white solid. R_f = 0 (c-Hex/EtOAc 1/1); **^{19}F NMR (CD_3OH, 564 MHz, 278 K)**: δ −88.8 (bs, 2F); IR (neat): υ_{max} 3279, 2961, 1647, 1524, 1451 cm^{-1}; (ESI-TOF, ion polarity positive): m/z $C_{46}H_{66}F_2N_{12}O_8S$ $[M+H]^+$ cal. 984.4815, found 984.4817; HPLC purity: XBridge C18 3.5 μm; H_2O + 0.2 % formic acid/ACN, gradient 5–100 % in 20 min; Rt = 12.41 min, 89 %. %. ^{1}H and ^{13}C NMR data are given in table 16–17S, SI. ^{1}H and ^{19}F spectra are respectively given in figures 40S and 43S, SI.

Boc-Asn(Trt)-NHCH$_2$CCH (11)

Following the general procedure **A** from L–Boc–Asn(Trt)–OH (1.0 g, 2.1 mmol) and propargylamine (126 mg, 2.3 mmol), the product **11** was obtained as a colorless solid (665 mg, 1.3 mmol, 62 %) and was used without further purification. mp = 76–78 °C; R_f = 0.3 (c-Hex/EtOAc: 7/3); IR: 3153, 2825, 1546, 1473, 1242, 1221, 1121, 1031, 970 cm^{-1}; Melting point: 76–78 °C; **^{1}H NMR (300 MHz, DMSO)**: δ 8.49 (s, 1H), 8.17 (t, ^3J = 5.6 Hz, 1H), 7.29–7.16 (m, 15H), 6.95 (t, ^3J = 8.4 Hz, 1H), 4.22 (bs, 1H), 3.84 (dd, ^3J = 5.6 Hz, ^4J = 2.5 Hz, 2H), 3.05 (t, ^4J = 2.5 Hz, 1H), 2.63 (dd, ^2J = 14.5 Hz, ^3J = 9.8 Hz, 1H), 1.39 (s, 9H);**^{13}C NMR (75 MHz, DMSO)**: δ 171.2, 168.9, 155.0, 144.7, 128.5, 127.4, 126.3, 81.0, 78.1, 72.8, 69.4, 51.6, 38.7, 28.2, 28.1.

Benzyl (2-azido-2,2-difluoroacetyl)-L-alaninate (12)

12 was obtained following the general procedure **B** from L-Alanine Benzyl ester hydrochloride (1.2 g, 5.6 mmol). The crude product obtained was purified by column chromatography (c-Hex/EtOAc: 92/8) to provide **12** (1.1 g, 3.8 mmol, 67 %) as a white solid. mp = 40–42 °C; R_f = 0.3 (c-Hex/EtOAc: 9/1); **^{1}H NMR (300 MHz, $CDCl_3$)**: δ 7.36 (m), 7.00 (s, 1H), 5.21 (s, 2H), 4.66–4.57, (m, 1H), 1.49 (d, ^3J = 7.1 Hz, 3H); **^{13}C NMR (75 MHz, $CDCl_3$)**: δ 171.4, 159.2 (t, ^2J(C, F) = 34.6 Hz), 134.9, 128.7, 128.3, 113.4 (t, ^1J(C, F) = 269.3 Hz), 67.8, 48.7, 17.8; **^{19}F NMR (188 MHz, $CDCl_3$)**: δ −82.98 (d, ^2J(F, F) = 194.5 Hz, 1F), −84.09 (d, ^2J(F, F) = 194.5 Hz, 1F); IR (neat): υ_{max} 3083, 2834, 1546, 1413, 1321, 1111, 1081, 930 cm^{-1}; **HRMS** (ESI-TOF, ion polarity positive): *m/z* $C_{12}H_{16}N_5O_3F_2$ $[M+NH_4]^+$ cal. 316.1221, found 316.1121.

BocNH-Phe-[TzlCF$_2$]-Ala-OBn Tetrapeptide (15)

The product was obtained following the general procedure **C** from **10** (500 mg, 1.7 mmol) and **12** (493 mg, 1.7 mmol). The crude product was purified by column chromatography (c-Hex/EtOAc: 65/35) to provide **15** (826 mg, 1.4 mmol, 81 %) as a white solid; Rf = 0.3 (c-Hex/EtOAc: 65/35); IR: 3213, 3001, 2954, 1593, 1501, 1252, 1211, 1141, 1013, 989 cm^{-1}; Melting point: 100–102 °C; **^{1}H NMR (300 MHz, $CDCl_3$)**: δ 7.87 (s, 1H), 7.37 (s, 5H), 7.17–7.13 (m, 5H), 6.50–6.39 (m, 1H), 5.23 (s, 2H), 4.99 (br s, 1H), 4.70 (t, ^3J = 7.2 Hz, 1H), 4.51 (d, ^3J = 5.9 Hz, 2H), 4.38–4.38 (m, 1H) 3.06 (d, 2H), 1.55 (d, ^3J =

7.2 Hz, 3H), 1.40 (s, 9H); **^{13}C NMR (75 MHz, $CDCl_3$)**: δ 172.5, 170.3, 157.9 (t, ^2J(C,F) = 31.3 Hz), 156.2, 145.5, 134.9, 128.7, 128.5, 120.9, 110.3 (t, ^1J(C,F) = 268.9 Hz), 80.3, 67.7, 55.9, 49.2, 39.9, 34.6, 28.3, 17.5; **^{19}F NMR (188 MHZ, $CDCl_3$)**: δ −86.8 (d, ^2J(F,F) = 209.9 Hz, 1F), −89.2 (d, ^2J(F,F) = 209.9 Hz, 1F); **HRMS** (ESI-TOF) *m/z* $C_{29}H_{38}N_7O_6F_2$ $[M+NH_4]^+$ cal. 618.2852, found 618.2855.

BocNH-Asn(Trt)-[TzlCF$_2$]-Phe-OBn Tetrapeptide (16)

The product was obtained following the general procedure **C** from **11** (600 mg, 1.2 mmol) and **13** (358 mg, 1.2 mmol). The crude product obtained was purified by column chromatography (CH_2Cl_2/MeOH: 99/1) to yield **16** (638 mg, 0.72 mmol, 60 %) as a white solid.; Rf = 0.4 (CH_2Cl_2/MeOH: 99/1); IR: 3252, 3111, 2910, 2904, 2873, 1598, 1512, 1443, 1212, 1102, 996 cm^{-1}; Melting point: 82–84 °C; **^{1}H NMR (300 MHz, $CDCl_3$)**: δ 7.87 (s, 1H), 7.38–7.17 (m, 25H), 7.04–7.00 (m, 3H), 6.00 (br s, 1H), 5.24 (d, ^2J = 11.8 Hz, 1H), 5.17 (d, ^2J = 12.1 Hz, 1H), 4.97 (q, ^3J = 6.5 Hz, 1H), 4.58–4.53 (m, 2H), 4.49–4.45 (m, 1H), 3.21 (d, ^3J = 5.3 Hz, 2H), 3.12 (dd, ^2J = 15.9 Hz, ^3J = 5.4 Hz, 1H), 2.61 (dd, ^2J = 15.9 Hz, ^3J = 5.4 Hz, 1H), 1.42 (s, 9H); **^{13}C NMR (75 MHz, $CDCl_3$)**:δ 171.6, 170.3, 169.7,157.5 (t, ^2J(C,F) = 31.1 Hz), 145.6, 144.2, 134.6, 134.5, 129.4, 128.8, 128.7, 128.6, 128.0, 127.4, 127.1, 120.8, 110.1 (t, ^1J(C,F) = 269.5 Hz), 80.5, 70.9, 67.9, 53.9, 51.5, 38.3, 37.3, 34.9, 28.3; **^{19}F NMR (188, MHz, $CDCl_3$)**: δ. −86.8 (d, ^2J(F,F) = 208.9 Hz, 1F) −88.7 (d, ^2J(F,F) = 208.9 Hz, 1F); **HRMS(ESI-TOF)** *m/z* $C_{49}H_{50}N_7O_7F_2$ $[M+H]^+$ cal. 886.3863, found 886.3869.

BocNH-[TzlCF$_2$]-Leu-NH$_2$ Tripeptide (17)

The product was obtained following the general procedure **C** from Boc-protected propargylamine (388 mg, 2.5 mmol) and **14** (623 mg, 2.5 mmol). The crude product was purified by column chromatography (c-Hex/EtOAc: 4/6) to provide **17** (727 mg, 1.8 mmol, 72 %) as a white solid.; Rf = 0.2 (c-Hex/EtOAc: 4/6); IR: 3144, 2914, 1614, 1554, 1413, 1240, 1100, 988 cm^{-1}; Melting point: 94–96 °C; **^{1}H NMR (200 MHz, $CDCl_3$)**: δ 7.94 (s, 1H), 7.72 (d, 1H), 6.54 (s, 1H), 5.75 (s, 1H), 5.23 (s, 1H) 4.58–4.47 (m, 1H,), 4.36 (d, ^3J = 5.7 Hz, 2H), 1.78 (m, 3H, 14), 1.37 (s, 9H), 0.91 (d, ^3J = 2.3 Hz, 3H), 0.88 (d, ^3J = 2.3 Hz, 3H); **^{13}C NMR (75 MHz, $CDCl_3$)**: δ 173.2, 158.1 (t, ^2J(C,F) = 31.2 Hz), 155.9, 146.6, 120.5, 110.3 (t, ^1J(C,F) = 268.4 Hz), 80.1, 52.4, 40.6, 35.8, 28.3, 24.8, 22.9, 21.6; **^{19}F NMR (188 MHz, $CDCl_3$)**: δ −86.0 (d, ^2J(F,F) = 205.5 Hz, 1F), −89.3 (d, ^2J(F,F) = 205.5 Hz, 1F); **HRMS** (ESI-TOF) *m/z* $C_{16}H_{27}N_6O_4F_2$ $[M+Na]^+$ cal. 405.2062, found 405.2068.

BocNH-[TzlCF$_2$]-Ala-OBn Tripeptide (18)

The product was obtained following the general procedure **C** from Boc-protected propargylamine (465 mg, 3.0 mmol) and **12** (894 mg, 3.0 mmol). The crude product was purified by column chromatography (c-Hex/EtOAc: 7/3) to yield **18** (1.0 mg, 2.3 mmol, 76 %) as a white solid.; Rf = 0.3 (c-Hex/EtOAc: 7/3); IR: 3102, 2923, 1601, 1542, 1243, 1222, 1107, 967 cm^{-1}; Melting point: 120–122 °C; **^{1}H NMR (300 MHz, $CDCl_3$)**: δ 7.97 (s, 1H), 7.63 (br s, 1H), 7.35 (s, 5H), 5.27 (m, 1H), 5.21 (s, 2H), 4.72–4.66 (m, 1H), 4.43–4.41 (m, 2), 1.53 (d, ^3J = 7.2 Hz, 3H), 1.44 (s, 9H); **^{13}C NMR (75 MHz, $CDCl_3$)**:δ 171.3, 157.6 (t, ^2J(C, F) = 32.5 Hz), 155.8, 146.2, 134.8, 128.7, 128.3, 120.6, 110.2 (t, ^1J(C, F) = 269.0 Hz) 80.2, 67.8, 49.1, 35.8, 28.3, 17.7; **^{19}F NMR (188, MHz, $CDCl_3$)**: δ. −87.1 (d, ^2J(F,F) = 210.3 Hz, 1F) −88.3 (d, ^2J(F,F) = 210.3 Hz, 1F); **HRMS**(ESI-TOF) *m/z* $C_{20}H_{26}N_5O_4F_2$ $[M+H]^+$ cal. 454.1810, found 454.1814.

BocNH-[TzlCF$_2$]-Ala-[TzlCF$_2$]-Leu-NH$_2$ Hexapeptide (19)

The product was obtained following the general procedure **D** from **18** (313 mg, 0.69 mmol) and **17** (279 mg, 0.69 mmol) which were both deprotected. The crude product obtained was purified by flash chromatography (CH_2Cl_2/MeOH: 99/1 to 90/10) to yield **19** (220 mg, 0.34 mmol, 49 %) as a white solid. Rf = 0.2 (CH_2Cl_2/MeOH: 95/5); IR: 3276, 3164, 3113, 2932, 2897, 1611, 1546, 1300, 1234 cm^{-1}; Melting point: 122–124 °C; **^{1}H NMR (200 MHz, CD_3OD)**:δ 8.39 (s, 1H), 8.34 (s, 1H), 4.57 (s, 2H), 4.53–4.50 (m, 2H), 4.37 (s, 1H), 1.74–1.72 (m, 3H), 1.49 (s, 3H), 1.44 (s, 9H); **^{13}C NMR (400 MHz, CD_3OD):δ** 176.0, 173.7, 148.1 (t, ^2J(C,F) = 30.7 Hz), 122.6, 122.2, 126.4, 111.9 (t, ^1J(F,F) = 267.3 Hz), 111.7 (t, ^1J(F,F) = 267.9 Hz), 53.8, 51.5, 41.4, 36.5, 35.7, 28.7, 26.0, 23.4, 21.6, 17.3; **^{19}F NMR (188 MHz, CD_3OD)**:δ −87.5 (d, ^2J(F,F) = 205.5 Hz, 1F), −87.7 (d, ^2J(F,F) = 205.5 Hz, 1F), −89.1 (d, ^2J(F,F) = 205.5 Hz, 1F), −89.2 (d, ^2J(F,F) = 205.5 Hz, 1F); **HRMS** (ESI-TOF) *m/z* $C_{24}H_{36}N_{11}O_6F_4$ $[M+H]^+$ cal. 650.2801, found 650.2795.

BocNH-Asn(Trt)-[TzlCF$_2$]-Phe-[TzlCF$_2$]-Ala-[TzlCF$_2$]-Leu-NH$_2$ Decapeptide (20)

20 was obtained following the general procedure **D** from **16** (284 mg, 0.32 mmol) and **19** (208 mg, 0.32 mmol) which were both deprotected. The crude product was purified by recrystallisation in MeOH to yield **20** (180 mg, 0.14 mmol, 42 %) as a white solid. mp = 112–114 °C; R_f = 0.2 (CH_2Cl_2/MeOH 93/7); **^{1}H NMR (400 MHz, DMSO-*d6*)**: δ 9.74 (brs, 1H), 9.69 (brs, 1H), 9.56 (d, ^3J = 8.2 Hz, 1H), 8.80 (t, ^3J = 5.3 Hz, 1H), 8.66 (t, ^3J = 5.6 Hz, 1H), 8.53 (bs, 1H), 8.51 (s, 1H), 8.43 (s, 1H), 8.41 (t, ^3J = 5.8 Hz, 1H), 8.13 (s, 1H), 7.48 (bs, 1H), 7.28–7.14 (m, 20H), 7.05 (d, ^3J = 7.9 Hz, 1H), 4.69–4.63 (m, 1H), 4.51–4.31 (m, 8H), 4.25–4.20 (m, 1H), 3.14 (dd, ^2J = 13.8 Hz ^3J = 4.8 Hz, 1H), 2.98 (dd, ^2J = 13.8 Hz ^3J = 4.8 Hz, 1H) 2.64 (dd, ^2J = 14.2 Hz ^3J = 9.5 Hz, 1H), 2.53 (dd, ^2J = 14.2 Hz ^3J = 9.5 Hz, 1H), 1.70–1.56 (m, 3H), 1.39 (s, 9H), 1.36 (d, ^3J = 7.2 Hz, 6H), 0.89 (d, ^3J = 6.3 Hz, 6H), 0.86 (d, ^3J = 6.3 Hz, 6H); **^{13}C NMR (400 MHz, DMSO-*d6*)**:δ 172.5, 171.7, 170.8, 169.6, 168.9, 157.5 (t, ^2J(C,F) = 30.9 Hz), 157.4 (t, ^2J(C,F) = 30.8 Hz), 155.2, 146.2, 145.8, 145.5, 144.7, 137.2, 129.0, 128.5, 128.1, 127.4, 126.4, 126.3, 121.7, 121.5, 121.2, 110.2 (t, ^1J(C,F) = 266.9 Hz), 110.1 (t, ^1J(C,F) = 266.2 Hz), 78.3, 69.4, 55.0, 52.0, 51.8, 49.3, 38.5, 36.7, 34.1, 34.0, 28.2, 24.2, 23.0, 21.1, 17.2; **^{19}F NMR (376 MHz, DMSO-*d6*)**: δ −85.7 (d, ^2J(F,F) = 205.0 Hz, 1F), −85.7 (d, ^2J(F,F) = 205.0 Hz, 1F), −85.3 (d, ^2J(F,F) = 205.0 Hz, 1F), −85.1 (d, ^2J(F,F) = 205.5 Hz, 1F), −84.3 (d, ^2J(F,F) = 205.0 Hz, 2F); **HRMS** (ESI-TOF, ion polarity positive): *m/z* $C_{61}H_{69}N_{18}O_{10}F_6$ $[M+H]^+$ cal. 1327.5308, found 1327.5311.

NMR Conformational Studies

Proton NMR spectra were recorded on Bruker spectrometers operating at 600 MHz, equipped with z-gradient TCI and ^{19}F-QCI cryoprobes (ICSN, Institut de Chimie des Substances Naturelles, Gif-sur-Yvette). ^{1}H and ^{13}C resonances were completely assigned using 1D ^{1}H WATERGATE, 2D ^{1}H–^{1}H TOCSY (mixing time set to 30, 60 or 100 ms), 2D ^{1}H–^{1}H ROESY (200 ms mixing time), 2D ^{1}H–^{13}C HSQC and 2D ^{1}H–^{13}C HMBC spectra, recorded at 278 K and 298 K (3 mM). ^{1}H and ^{13}C chemical shifts were calibrated using the solvent residual peak (CD_3OH, δ ^{1}H 3.31 ppm). The chemical shift deviations were calculated as the differences between observed chemical shifts and random coil values reported in water reported by Wishart *et al.* (^{1}H, ^{13}C, and ^{15}N random coil NMR chemical shifts of the common amino acids). Vicinal coupling constants were extracted from the 1D ^{1}H spectrum and 2D ^{1}H–^{1}H COSY at 283 K and 313 K. Temperature coefficient ($\Delta\delta_{HN}/\Delta T$) of the amide protons were calculated between 283–313 K.

Computational Methods

4/**5** and **6**/**7** three-dimensional structures were generated using MarvinSketch 6.2.1 from ChemAxon (https://www.chemaxon.com/). Each compound was placed in a cubic simulation box so that the minimum distance between the solute and the cube sides was 1.4 nm. Simulation boxes were subsequently filled with explicit methanol molecules. The SPC/E model was used for water.[85] Molecular dynamics simulations were performed by using the GROMACS 2019.1 package[86] with the Generalized AMBER Force Field (GAFF)[87] for both solute and methanol solvent. The length of the covalent bonds involving hydrogens was kept constant using the LINCS procedure.[88] Lennard-Jones potentials were cut-off at 1.2 nm and electrostatic interactions were treated using the smooth PME method.[89] After two short simulations of 1 ns each to bring the temperature and pressure around T = 300 K and P = 1 bar, each system was simulated during 500 ns in the isothermal-isobaric ensemble using the Nose-Hoover[90,91] and Parrinello-Rahman[92] coupling methods. Molecule coordinates were saved every 20 ps for subsequent analyses by the *gmx cluster* and *gmx mindist* GROMACS tools.

Fluorescence-Detected ThT Binding Assay (hIAPP)

hIAPP, purchased from Bachem, was dissolved in pure hexafluoroisopropanol (HFIP) at a concentration of 1 mM and incubated for 1 hour at room temperature to dissolve any preformed aggregates. Next, HFIP was evaporated with dry nitrogen gas followed by vacuum desiccation for 3 hours. The resulting peptide film was then dissolved in DMSO to obtain stock solutions of hIAPP (0.2 mM). Stock solutions of foldamers were dissolved in DMSO or water (10, 1, and 0.1 mM). The concentration of DMSO was kept constant at 3% (v/v) in the final volume of 200 μL. Thioflavin-T binding assays were used to measure the formation of fibrils over time. A plate reader (Fluostar Optima, BmgLabtech) and standard 96-wells flat-bottom black microtiter plates in combination with 440 nm excitation and 480 nm emission filters were used. The ThT assay was started by adding 5 μL of a 0.2 mM hIAPP stock solution to a mixture of 10 μM ThT and 10 mM Tris/HCl, 100 mM NaCl at pH 7.4 containing 1 μL of stock solutions of foldamers. The concentration of IAPP was held constant at 5 μM and foldamers were added to yield foldamer/IAPP ratios of 10/1, 1/1, and 0.1/1. The ThT assays were performed in triplicate and between 2 and 4 times on different days, with the same batch of peptide. The ability of foldamers to inhibit hIAPP aggregation was assessed considering the time of the half-aggregation (*t1/2*) and the intensity of the experimental fluorescence plateau (F), both values were obtained by fitting the obtained kinetic data of one assay (n = 3) to a Boltzmann sigmoidal curve using GraphPad Prism 5. The relative extension/reduction of *t1/2* is defined as the experimental *t1/2* in the presence of the tested compound relative to the one obtained without the compound and is evaluated as the following percentage: [*t1/2* (hIAPP + compound) − *t1/2* (hIAPP)]/*t1/2* (hIAPP) ×100. The relative extension/reduction of the experimental plateau is defined as the intensity of the experimental fluorescence plateau observed with the tested compound relative to the value obtained without the compound and is evaluated as the following percentage: (F hIAPP + compound − F hIAPP)/F hIAPP×100. Curves of the tested compounds are fitted to a Boltzmann sigmoidal model, normalized to the maximal fluorescence of the control experiment, and represented in supporting information for **1**–**9**, $FGAILNH_2$, and $NNFGAILNH_2$ (Figure 52S, SI).

ESI-MS experiments were carried out with a Synapt G2-S^i Q-TOF instrument (Waters, Manchester, UK) equipped with an ESI interface. Positive ion mode was used. Samples of hIAPP (pretreated with HFIP as previously described for the fluorescence-detected ThT binding assay) were reconstituted in 50 mM ammonium acetate buffer pH 3.7 at 100 μM. Compounds **1**, **5**, and **7** were dissolved in DMSO and added to the peptide solution to reach final concentrations of 1 mM, 500, and 10 μM, corresponding respectively to ratios 10/1, 5/1, and 1/1 of compounds/hIAPP; the final concentration of DMSO in the ammonium acetate buffer being of 5% (v/v). Samples were injected by direct infusion through a syringe at 5μL/min. The main MS parameters are detailed the follows: the capillary voltage was set at 2.4 kV, with the sampling cone and source offset at 70 V. Source and desolvation temperatures were respectively 40 °C and 75 °C. Data were processed with MassLynx.

Ion mobility experiments were performed using a Travelling Wave Ion Mobility device, equipped on the G2-Si Q-TOF. Briefly, ion mobility parameters were: Trap gas flow = 7 ml/min; Helium gas flow120, IMS gas flow = 45, IMS wave velocity = 110 m/sec, wave height 40 V. Ion mobility data were similarly processed using MassLynx™ software.

NMR Experiments

Synthetic human-IAPP peptide was purchased from AnaSpec at > 95% purity. The peptide was used without any further purification. It was dissolved in hexafluoroisopropanol (HFIP) and kept on ice for 30 minutes. HFIP treated peptide aliquots each containing 0.1 mg of human-IAPP were next subjected to lyophilization for 24 hours. The lyophilized hIAPP peptide was dissolved in d11–10 mM TRIS, 100 mM NaCl, pH 7.4 (or d3–30 mM sodium acetate buffer, pH 5.5) as required for biophysical measurements. Uniformly-^{15}N-labelled hIAPP was biologically expressed and purified.[93] ^{15}N-hIAPP peptide samples were prepared in the same way as the unlabeled peptides.

Proton and ^{19}F NMR spectra were recorded on a 500 MHz Bruker NMR spectrometer equipped with a z-axis gradient triple-resonance probe (^{1}H/^{19}F/^{13}C). 2D SOFAST-HMQC spectra of uniformly ^{15}N labelled hIAPP peptide were recorded on an 800 MHz Bruker spectrometer equipped with a cryoprobe. Proton NMR spectra of 50 μM of unlabeled hIAPP were recorded in the absence and presence of 5 molar excess of **1**/**5**. The NMR sample was prepared in 10 mM Tris, 100 mM NaCl, pH 7.4 buffer containing 87.5% H_2O, 10% D_2O, and 2.5% DMSO-d_6. 2D SOFAST-HMQC spectra were recorded for 70 μM of uniformly-15 N-labelled hIAPP in the absence and presence of 5 molar excess of **1** or **5**. The NMR sample for SOFAST-HMQC measurement was prepared in 30 mM d3-sodium acetate buffer, pH 5.5 containing 87.5% H_2O, 10% D_2O, and 2.5% DMSO-d_6. 2D SOFAST-HMQC spectra were acquired at 25 °C with 32 scans and 128 t1 increments. ^{1}H, ^{19}F, and 2D SOFAST-HMQC NMR spectra were processed using TopSpin 3.5 (Bruker) and the 2D SOFAST-HMQC spectra were analyzed using Sparky. The ^{19}F signal intensities were calculated using the Mestrelab MNova program.

Acknowledgements

The Ministère de l'Enseignement Supérieur et de la Recherche (MESR) is thanked for financial support for José Laxio Arenas and Jacopo Lesma. We thank Giovanna Cardella (Erasmus student from Università degli studi di Milano) for her help in the final steps of the synthesis of compounds **6** and **7**, and Dr. Saba Suladze and Prof. Dr. Bernd Reif from the Technical University of Munich, Germany, for the production of ^{15}N-labeled human-IAPP.

Conflict of Interests

No conflict to declare.

Data Availability Statement

The data that support the findings of this study are available from the corresponding author upon reasonable request.

Keywords: amyloid · aggregation · foldamer · peptidomimetic · beta-hairpin · triazole · fluorine

[1] P. C. Ke, R. Zhou, L. C. Serpell, R. Riek, T. P. J. Knowles, H. A. Lashuel, E. Gazit, I. W. Hamley, T. P. Davis, M. Fändrich, D. E. Otzen, M. R. Chapman, C. M. Dobson, D. S. Eisenberg, R. Mezzenga, *Chem. Soc. Rev.* **2020**, *49*, 5473–5509.
[2] P. C. Ke, M.-A. Sani, F. Ding, A. Kakinen, I. Javed, F. Separovic, T. P. Davis, R. Mezzenga, *Chem. Soc. Rev.* **2017**, *46*, 6492–6531.
[3] P. H. Nguyen, A. Ramamoorthy, B. R. Sahoo, J. Zheng, P. Faller, J. E. Straub, L. Dominguez, J.-E. Shea, N. V. Dokholyan, A. De Simone, B. Ma, R. Nussinov, S. Najafi, S. T. Ngo, A. Loquet, M. Chiricotto, P. Ganguly, J. McCarty, M. S. Li, C. Hall, Y. Wang, Y. Miller, S. Melchionna, B. Habenstein, S. Timr, J. Chen, B. Hnath, B. Strodel, R. Kayed, S. Lesné, G. Wei, F. Sterpone, A. J. Doig, P. Derreumaux, *Chem. Rev.* **2021**, *121*, 2545–2647.
[4] A. Chaudhury, C. Duvoor, V. S. Reddy Dendi, S. Kraleti, A. Chada, R. Ravilla, A. Marco, N. S. Shekhawat, M. T. Montales, K. Kuriakose, A. Sasapu, A. Beebe, N. Patil, C. K. Musham, G. P. Lohani, W. Mirza, *Front. Endocrinol.* **2017**, *8*, 6.
[5] IDF Diabetes Atlas 9th edition 2019, https://www.diabetesatlas.org/en/ (accessed October 15, 2023).
[6] R. Akter, P. Cao, H. Noor, Z. Ridgway, L.-H. Tu, H. Wang, A. G. Wong, X. Zhang, A. Abedini, A. M. Schmidt, D. P. Raleigh, *J. Diabetes Res.* **2016**, *2016*, 1–18.
[7] S. S. An, H. R. Jeong, *Clin. Interventions Aging* **2015**, *10*, 1873–1879.
[8] Y. Kiriyama, H. Nochi, *Cells* **2018**, *7*, 95.
[9] Y. Bram, A. Frydman-Marom, I. Yanai, S. Gilead, R. Shaltiel-Karyo, N. Amdursky, E. Gazit, *Sci. Rep.* **2014**, *4*, 4267.
[10] J. R. Brender, S. Salamekh, A. Ramamoorthy, *Acc. Chem. Res.* **2012**, *45*, 454–462.
[11] M. S. Terakawa, Y. Lin, M. Kinoshita, S. Kanemura, D. Itoh, T. Sugiki, M. Okumura, A. Ramamoorthy, Y.-H. Lee, *Biochim. Biophys. Acta Biomembr.* **2018**, *1860*, 1741–1764.
[12] S. J. Cox, D. C. Rodriguez Camargo, Y.-H. Lee, R. C. A. Dubini, P. Rovo, M. I. Ivanova, V. Padmini, B. Reif, A. Ramamoorthy, *Chem. Commun.* **2020**, *56*, 13129–13132.
[13] D. Milardi, E. Gazit, S. E. Radford, Y. Xu, R. U. Gallardo, A. Caflisch, G. T. Westermark, P. Westermark, C. L. Rosa, A. Ramamoorthy, *Chem. Rev.* **2021**, *121*, 1845–1893.
[14] A. Pithadia, J. R. Brender, C. A. Fierke, A. Ramamoorthy, *J. Diabetes Res.* **2016**, *2016*, 2046327.
[15] M. S. Saravanan, S. Ryazanov, A. Leonov, J. Nicolai, P. Praest, A. Giese, R. Winter, L. Khemtemourian, C. Griesinger, J. A. Killian, *Sci. Rep.* **2019**, *9*, 19023.
[16] V. Armiento, A. Spanopoulou, A. Kapurniotu, *Angew. Chem. Int. Ed. Engl.* **2020**, *59*, 3372–3384.
[17] P.-N. Cheng, C. Liu, M. Zhao, D. Eisenberg, J. S. Nowick, *Nat. Chem.* **2012**, *4*, 927–933.
[18] S. Gilead, E. Gazit, *Angew. Chem. Int. Ed. Engl.* **2004**, *43*, 4041–4044.
[19] A. Paul, S. Kalita, S. Kalita, P. Sukumar, B. Mandal, *Sci. Rep.* **2017**, *7*, 40095.
[20] S. H. Gellman, *Acc. Chem. Res.* **1998**, *31*, 173–180.
[21] G. Guichard, I. Huc, *Chem. Commun.* **2011**, *47*, 5933–5941.
[22] T. A. Martinek, F. Fülöp, *Chem. Soc. Rev.* **2012**, *41*, 687–702.
[23] R. Gopalakrishnan, A. I. Frolov, L. Knerr, W. J. Drury, E. Valeur, *J. Med. Chem.* **2016**, *59*, 9599–9621.
[24] I. M. Mándity, F. Fülöp, *Expert Opin. Drug Discovery* **2015**, *10*, 1163–1177.
[25] S. Kumar, A. Henning-Knechtel, I. Chehade, M. Magzoub, A. D. Hamilton, *J. Am. Chem. Soc.* **2017**, *139*, 17098–17108.
[26] S. Kumar, A. D. Hamilton, *J. Am. Chem. Soc.* **2017**, *139*, 5744–5755.
[27] S. Kumar, A. D. Miranker, *Chem. Commun. (Camb.)* **2013**, *49*, 4749–4751.
[28] S. Kumar, M. Birol, D. E. Schlamadinger, S. P. Wojcik, E. Rhoades, A. D. Miranker, *Nat. Commun.* **2016**, *7*, 11412.
[29] J. Kaffy, C. Berardet, L. Mathieu, B. Legrand, M. Taverna, F. Halgand, G. V. D. Rest, L. T. Maillard, S. Ongeri, *Chem. Eur. J.* **2020**, *26*, 14612–14622.
[30] C. Shi, J. Kaffy, T. Ha-Duong, J. F. Gallard, A. Pruvost, A. Mabondzo, L. Ciccone, S. Ongeri, N. Tonali, *J. Med. Chem.* **2023**, *66*, 12005–12017.
[31] A. Hassoun, C. M. Grison, R. Guillot, T. Boddaert, D. J. Aitken, *New J. Chem.* **2015**, *39*, 3270–3279.
[32] D. Gimenez, J. A. Aguilar, E. H. C. Bromley, S. L. Cobb, *Angew. Chem. Int. Ed.* **2018**, *57*, 10549–10553.
[33] J. Cho, K. Sawaki, S. Hanashima, Y. Yamaguchi, M. Shiro, K. Saigo, Y. Ishida, *Chem. Commun.* **2014**, *50*, 9855–9858.
[34] C.-F. Wu, Z.-M. Li, X.-N. Xu, Z.-X. Zhao, X. Zhao, R.-X. Wang, Z.-T. Li, *Chem. Eur. J.* **2014**, *20*, 1418–1426.
[35] A. Ueda, M. Ikeda, T. Kasae, M. Doi, Y. Demizu, M. Oba, M. Tanaka, *ChemistrySelect* **2020**, *5*, 10882–10886.
[36] L. Bodero, K. Guitot, N. Lensen, O. Lequin, T. Brigaud, S. Ongeri, G. Chaume, *Chem. Eur. J.* **2022**, *28*, e202103887.
[37] Y. Zhou, J. Wang, Z. Gu, S. Wang, W. Zhu, J. L. Aceña, V. A. Soloshonok, K. Izawa, H. Liu, *Chem. Rev.* **2016**, *116*, 422–518.
[38] M. Inoue, Y. Sumii, N. Shibata, *ACS Omega* **2020**, *5*, 10633–10640.
[39] A. A. Berger, J.-S. Völler, N. Budisa, B. Koksch, *Acc. Chem. Res.* **2017**, *50*, 2093–2103.
[40] H. Mei, J. Han, K. D. Klika, K. Izawa, T. Sato, N. A. Meanwell, V. A. Soloshonok, *Eur. J. Med. Chem.* **2020**, *186*, 111826.
[41] J. Moschner, V. Stulberg, R. Fernandes, S. Huhmann, J. Leppkes, B. Koksch, *Chem. Rev.* **2019**, *119*, 10718–10801.
[42] S. Huhmann, B. Koksch, *Eur. J. Org. Chem.* **2018**, 3667–3679.
[43] M. Mamone, R. S. B. Gonçalves, F. Blanchard, G. Bernadat, S. Ongeri, T. Milcent, B. Crousse, *Chem. Commun.* **2017**, *53*, 5024–5027.
[44] J. Laxio Arenas, Y. Xu, T. Milcent, C. V. Heijenoort, F. Giraud, T. Ha-Duong, B. Crousse, S. Ongeri, *ChemPlusChem* **2021**, *86*, 241–251.
[45] H. C. Kolb, M. G. Finn, K. B. Sharpless, *Angew. Chem. Int. Ed.* **2001**, *40*, 2004–2021.
[46] C. W. Tornøe, C. Christensen, M. Meldal, *J. Org. Chem.* **2002**, *67*, 3057–3064.
[47] W. S. Horne, *Expert Opin. Drug Discovery* **2011**, *6*, 1247–1262.
[48] K. B. H. Salah, S. Das, N. Ruiz, V. Andreu, J. Martinez, E. Wenger, M. Amblard, C. Didierjean, B. Legrand, N. Inguimbert, *Org. Biomol. Chem.* **2018**, *16*, 3576–3583.
[49] S. S. Bag, S. Jana, A. Yashmeen, S. De, *Chem. Commun.* **2015**, *51*, 5242–5245.
[50] K. Oh, Z. Guan, *Chem. Commun.* **2006**, *29*, 3069–3071.
[51] N. Tonali, L. Hericks, D. C. Schröder, O. Kracker, R. Krzemieniecki, J. Kaffy, V. L. Joncour, P. Laakkonen, A. Marion, S. Ongeri, V. I. Dodero, N. Sewald, *ChemPlusChem* **2021**, *86*, 840–851.
[52] Z. Ke, H.-F. Chow, M.-C. Chan, Z. Liu, K.-H. Sze, *Org. Lett.* **2012**, *14*, 394–397.
[53] N. G. Angelo, P. S. Arora, *J. Am. Chem. Soc.* **2005**, *127*, 17134–17135.
[54] D. C. Schröder, O. Kracker, T. Fröhr, J. Góra, M. Jewginski, A. Nieß, I. Antes, R. Latajka, A. Marion, N. Sewald, *Front. Chem.* **2019**, *7*, 155.
[55] J. Lesma, F. Bizet, C. Berardet, N. Tonali, S. Pellegrino, M. Taverna, L. Khemtemourian, J.-L. Soulier, C. van Heijenoort, F. Halgand, T. Ha-Duong, J. Kaffy, S. Ongeri, *Front. Cell Dev. Biol.* **2021**, *9*, 2531.
[56] Q. Cao, D. R. Boyer, M. R. Sawaya, P. Ge, D. S. Eisenberg, *Nat. Struct. Mol. Biol.* **2020**, *27*, 653–659.
[57] C. Wu, J.-E. Shea, *PLoS Comput. Biol.* **2013**, *9*, e1003211.
[58] T. Linh, H.-D. Tap, *Curr. Pharm. Des.* **2016**, *22*, 3601–3607.
[59] C. Röder, T. Kupreichyk, L. Gremer, L. U. Schäfer, K. R. Pothula, R. B. G. Ravelli, D. Willbold, W. Hoyer, G. F. Schröder, *Nat. Struct. Mol. Biol.* **2020**, *27*, 660–667.
[60] G. G. Glenner, E. D. Eanes, C. A. Wiley, *Biochem. Biophys. Res. Commun.* **1988**, *155*, 608–614.
[61] C. Betsholtz, L. Christmansson, U. Engström, F. Rorsman, V. Svensson, K. H. Johnson, P. Westermark, *FEBS Lett.* **1989**, *251*, 261–264.
[62] J. J. W. Wiltzius, S. A. Sievers, M. R. Sawaya, D. Cascio, D. Popov, C. Riekel, D. Eisenberg, *Protein Sci. Publ. Protein Soc.* **2008**, *17*, 1467–1474.
[63] L. A. Scrocchi, Y. Chen, S. Waschuk, F. Wang, S. Cheung, A. A. Darabie, J. McLaurin, P. E. Fraser, *J. Mol. Biol.* **2002**, *318*, 697–706.
[64] L. E. Buchanan, E. B. Dunkelberger, H. Q. Tran, P.-N. Cheng, C.-C. Chiu, P. Cao, D. P. Raleigh, J. J. de Pablo, J. S. Nowick, M. T. Zanni, *Proc. Nat. Acad. Sci.* **2013**, *110*, 19285–19290.

[65] M. Tatarek-Nossol, L.-M. Yan, A. Schmauder, K. Tenidis, G. Westermark, A. Kapurniotu, *Chem. Biol.* **2005**, *12*, 797–809.
[66] E. Andreetto, E. Malideli, L.-M. Yan, M. Kracklauer, K. Farbiarz, M. Tatarek-Nossol, G. Rammes, E. Prade, T. Neumüller, A. Caporale, A. Spanopoulou, M. Bakou, B. Reif, A. Kapurniotu, *Angew. Chem. Int. Ed. Engl.* **2015**, *54*, 13095–13100.
[67] Z. Niu, E. Prade, E. Malideli, K. Hille, A. Jussupow, Y. G. Mideksa, L.-M. Yan, C. Qian, M. Fleisch, A. C. Messias, R. Sarkar, M. Sattler, D. C. Lamb, M. J. Feige, C. Camilloni, A. Kapurniotu, B. Reif, *Angew. Chem. Int. Ed.* **2020**, *59*, 5771–5781.
[68] P. K. Mandal, J. S. McMurray, *J. Org. Chem.* **2007**, *72*, 6599–6601.
[69] S. Pellegrino, A. Contini, M. L. Gelmi, L. Lo Presti, R. Soave, E. Erba, *J. Org. Chem.* **2014**, *79*, 3094–3102.
[70] S. Pellegrino, N. Tonali, E. Erba, J. Kaffy, M. Taverna, A. Contini, M. Taylor, D. Allsop, M. L. Gelmi, S. Ongeri, *Chem. Sci.* **2017**, *8*, 1295–1302.
[71] N. Tonali, J. Kaffy, J.-L. Soulier, M. L. Gelmi, E. Erba, M. Taverna, C. van Heijenoort, T. Ha-Duong, S. Ongeri, *Eur. J. Med. Chem.* **2018**, *154*, 280–293.
[72] L. J. Smith, K. A. Bolin, H. Schwalbe, M. W. MacArthur, J. M. Thornton, C. M. Dobson, *J. Mol. Biol.* **1996**, *255*, 494–506.
[73] H. LeVine, *Methods Enzymol.* **1999**, *309*, 274–284.
[74] K. Gade Malmos, L. M. Blancas-Mejia, B. Weber, J. Buchner, M. Ramirez-Alvarado, H. Naiki, D. Otzen, *Amyloid* **2017**, *24*, 1–16.
[75] J. Hu, Q. Zheng, *Front. Chem.* **2020**, *8*, 324.
[76] C. Berardet, J. Kaffy, F. Halgand, G. Van der Rest, S. Ongeri, M. Taverna, *Anal. Bioanal. Chem.* **2020**, *412*, 3103–3111.
[77] L. M. Young, P. Cao, D. P. Raleigh, A. E. Ashcroft, S. E. Radford, *J. Am. Chem. Soc.* **2014**, *136*, 660–670.
[78] L. M. Young, J. C. Saunders, R. A. Mahood, C. H. Revill, R. J. Foster, L.-H. Tu, D. P. Raleigh, S. E. Radford, A. E. Ashcroft, *Nat. Chem.* **2015** *7*, 73–81.
[79] I. Riba, P. E. Barran, G. J. S. Cooper, R. D. Unwin, *Int. J. Mass Spectrom.* **2015**, *391*, 47–53.
[80] H. Li, E. Ha, R. P. Donaldson, A. M. Jeremic, A. Vertes, *Anal. Chem.* **2015**, *87*, 9829–9837.
[81] L. M. Young, J. C. Saunders, R. A. Mahood, C. H. Revill, R. J. Foster, A. E. Ashcroft, S. E. Radford, *Methods* **2016**, *95*, 62–69.
[82] P. Bharadwaj, T. Solomon, B. R. Sahoo, K. Ignasiak, S. Gaskin, J. Rowles, G. Verdile, M. J. Howard, C. S. Bond, A. Ramamoorthy, R. N. Martins, P. Newsholme, *Sci. Rep.* **2020**, *10*, 10356.
[83] D. Gimenez, A. Phelan, C. D. Murphy, S. L. Cobb, *Beilstein J. Org. Chem.* **2021**, *17*, 293–318.
[84] C. Dalvit, A. Vulpetti, *J. Med. Chem.* **2019**, *62*, 2218–2244.
[85] H. J. C. Berendsen, J. R. Grigera, T. P. Straatsma, *J. Phys. Chem.* **1987**, *91*, 6269–6271.
[86] M. J. Abraham, T. Murtola, R. Schulz, S. Páll, J. C. Smith, B. Hess, E. Lindahl, *SoftwareX* **2015**, *1–2*, 19–25.
[87] J. Wang, R. M. Wolf, J. W. Caldwell, P. A. Kollman, D. A. Case, *J. Comput. Chem.* **2004**, *25*, 1157–1174.
[88] B. Hess, *J. Chem. Theory Comput.* **2008**, *4*, 116–122.
[89] U. Essmann, L. Perera, M. L. Berkowitz, T. Darden, H. Lee, L. G. Pedersen, *J. Chem. Phys.* **1995**, *103*, 8577–8593.
[90] S. Nosé, *J. Chem. Phys.* **1984**, *81*, 511–519.
[91] W. G. Hoover, *Phys. Rev. A* **1985**, *31*, 1695–1697.
[92] M. Parrinello, A. Rahman, *J. Appl. Phys.* **1981**, *52*, 7182–7190.
[93] D. C. Rodriguez, Camargo, K. Tripsianes, K. Buday, A. Franko, C. Göbl, C. Hartlmüller, R. Sarkar, M. Aichler, G. Mettenleiter, M. Schulz, A. Böddrich, C. Erck, H. Martens, A. K. Walch, T. Madl, E. E. Wanker, M. Conrad, M. H. de Angelis, B. Reif, *Sci. Rep.* **2017**, *7*, 44041.

Manuscript received: November 22, 2023
Accepted manuscript online: March 13, 2024
Version of record online: ■■, ■■

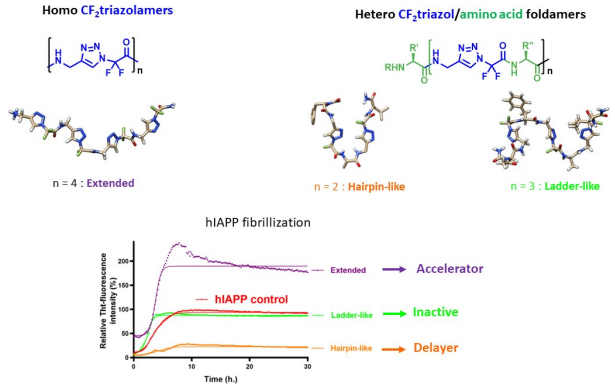

While fluorinated molecules constitute nearly 30% of all newly approved drugs, and peptidomimetic foldamers provide original solutions to resolve certain peptide problems, the interest of fluorinated foldamers is still little addressed. The conformational and biological interest of fluorinated triazolamers as an alternative to natural peptides is demonstrated here.

Dr. J. Laxio Arenas, Dr. J. Lesma, Prof. T. Ha-Duong, Dr. B. Ranjan Sahoo, Prof. A. Ramamoorthy, Dr. N. Tonali, Dr. J.-L. Soulier, Dr. F. Halgand, F. Giraud, Dr. B. Crousse, J. Kaffy, Prof. S. Ongeri**

1 – 20

Composition and Conformation of Hetero- *versus* Homo-Fluorinated Triazolamers Influence their Activity on Islet Amyloid Polypeptide Aggregation